2.5. *In vitro differentiation analysis of sphere-initiating cells in the FA+/dNS− or FA−/dNS+ media*

To examine the multipotency of spheres under the FA+/dNS− and FA−/dNS+ conditions, we transferred and placed isolated spheres under the differentiation condition. After 4 DIV of differentiation, triple-labeled immunocytochemistry for tubulin β III, GFAP, and O4 revealed that cells with the morphological and antigenic characteristics of neurons, astrocytes, and oligodendrocytes, respectively, were generated from the FA+/dNS− spheres (Figs. 5A, C–F). In contrast, the FA−/dNS+ spheres yielded astrocytes and oligodendrocytes, but neither tubulin β III nor MAP2 positive neurons (Figs. 5B, G–I). The percentage of tubulin β III positive neurons that differentiated from the FA−/dNS+ primary spheres was 0.067% ± 0.009% (n = 4) significantly lower than that from the FA+/dNS− primary spheres (6.618% ± 0.188%, n = 5, $P < 0.01$), as well as the percentage of tubulin β III positive neurons from secondary spheres (FA−/dNS+, 0.035% ± 0.004% vs. FA+/dNS−, 9.81% ± 1.516%, n = 4, $P < 0.01$) (Fig. 5J). According to previous studies, the percentage of neurons derived from the neurosphere culture under the regular condition was 5%–10% (Laeng et al., 2004; Palmer et al., 1999). These results suggested that spheres formed under the FA+/dNS− condition, but not under the FA−/dNS+ condition, coincided with the definition of a neurosphere, self-renewal capability, and multipotency (Seaberg and van der Kooy, 2002).

2.6. *Effects of inhibitors of de novo DNA synthesis on in vitro differentiation*

We hypothesized that the disturbance of de novo DNA synthesis in the sphere-forming neural stem cells resulted in the decrease of neurons. To test the hypothesis, we added de novo synthesis inhibitors to the FA+/dNS+ medium. AZP blocks the conversion of inosinate to adenyl succinate, which is the key reaction in the formation of purine adenylate; additionally, it also blocks an important step in the production of the purine base guanylate (Belgi and Friedmann, 2002) (Fig. 1). MTX is a competitive inhibitor of dihydrofolate reductase (EC 1.5.1.3), which generates tetrahydrofolate from dihydrofolate. As a result, MTX interferes with the conversion of deoxyuridylate to thymidylate in the synthesis of DNA (Olsen, 1991) (Fig. 1). Both AZP and MTX inhibited sphere formation in a dose-dependent manner (Figs. 6A–C). The inhibition was most evident under the FA+/NS− condition. These results suggested that lower doses of AZP and MTX (e.g., <1 μM) selectively inhibited the de novo DNA synthesis in sphere-forming cells. We transferred the spheres obtained under these conditions and placed them under the differentiation condition (Fig. 6D). After 4 DIV, the percentage of tubulin β III positive neurons derived from the FA+/dNS+ spheres significantly (n = 4, $P < 0.01$) decreased in the presence of AZP or MTX (Fig. 6E). Figs. 6F–I show representative fields of the culture under the FA+/dNS+ condition (Fig. 6F), FA−/dNS+ condition (Fig. 6G), FA+/dNS+ with 1 μM AZP condition (Fig. 6H), and FA+/dNS+ with 0.1 μM MTX condition (Fig. 6I). The number of astrocytes did not significantly differ among these conditions (data not shown).

3. Discussion

We performed the neurosphere method by using modified media that lacked FA or dNS and added specific inhibitors of DNA synthesis. Cultured cells barely proliferated and underwent apoptosis under the FA−/dNS− condition. Although sphere formation was observed, the spheres formed under the FA−/dNS+ condition poorly produced neurons. Since extracellular nucleosides exert various effects on cell differentiation, apoptosis, mitogenesis, and stimulators of cytokine release in the nervous system (Neary et al., 1996), the decreased percentage of neurons derived from the FA−/dNS+ spheres could be attributed to the effects of extracellular nucleosides. However, there was no significant difference ($P > 0.05$) between the percentage of neurons derived from FA+/dNS+ spheres (7.662 ± 1.672%, n = 4) (Fig. 6E) and FA+/NS− spheres (6.618% ± 0.188%, n = 5) (Fig. 5J). Addition of inhibitors of de novo DNA synthesis, namely, AZP and MTX, resulted in poor neuronal differentiation even under the FA+/dNS+ condition. Taken together, low percentage of neurons derived from spheres formed under the FA−/dNS+ condition is not due to the extracellular effects of dNS, but due to the proliferation failure of sphere-forming neural stem cells induced by inactivation of the de novo DNA synthesis pathway.

The neurosphere cultures established from the E12.5 mouse proliferated to a lesser extent than those obtained from the E14.5 or E16.5 mouse under the FA−/dNS+ condition, while they proliferated to an equivalent extent under the FA+/dNS− condition. As shown in the differentiation assay, FA−/dNS+ spheres were likely to consist of cells committed to the glial lineage (Seaberg and van der Kooy, 2002). This result may be in line with the fact that neurogenesis precedes gliogenesis (Qian et al., 2000). To clarify the mechanism responsible for the developmental change in the DNA synthesis pathway, we compared the mRNA expression of thymidine kinase (EC. 2.7.1.21), deoxycytidine kinase (EC. 2.7.1.74), and adenosine kinase (EC. 2.7.1.45)—key enzymes for the salvage pathway (Karbownik et al., 2003)—and that of thymidylate synthetase (EC. 2.1.1.45)—a key enzyme for the de novo pathway (Chu et al., 2003)—in the E11.5 and E16.5 mouse neuroepithelium. There was no detectable change in semi-quantitative RT-PCR (data not shown). The activities of several key enzymes involved in DNA synthesis were previously reported using developmental brain tissues (Hyndman and Zamenhof, 1978; Suleiman and Spector, 1982; Sung, 1971). These reports suggested that the specific activities of both the DNA synthesis pathways equally decreased in proportion with maturation. Since there is a discrepancy between the mRNA levels and enzymatic activities, the activities of the key enzymes involved in the DNA synthesis pathways may also be regulated translationally and/or posttranslationally (Ayusawa et al., 1986; Sherley and Kelly, 1988).

FA is a cofactor in one-carbon metabolism, and it promotes the remethylation of homocysteine. Folate deficiency allows the accumulation of intracellular homocysteine, a potentially neurotoxic amino acid that can induce DNA strand break, thereby triggering apoptosis (Mattson

and Shea, 2003). FA deficiency and elevated homocysteine levels endanger postmitotic neurons in neurodegenerative disease model mice (Duan et al., 2002; Kruman et al., 2002). To test the effect of homocysteine on sphere-forming neural stem cells, we performed a neurosphere assay in the FA+/dNS+ medium supplemented with 0.1–1000 μM homocysteine. However, no toxic effect was observed with any concentration of homocysteine. Additionally, no inhibitory effect of homocysteine on neuronal differentiation was observed in the in vitro differentiation assay (unpublished data). These results suggest that the high concentration of homocysteine due to FA deficiency cannot explain the proliferation failure of neural stem cells observed in our study.

De novo DNA synthesis inhibitors, such as MTX and AZP, are reported to induce selective malformation of the rhombencephalic and telencephalic brain regions in rat embryo cultures (Schmid, 1984) and neural tube defects (NTD) in rabbits (Lloyd et al., 1999). In humans, NTD can be prevented by FA supplementation in the periconceptual period (Czeizel and Dudas, 1992; Daly et al., 1995). Although FA deficiency does not cause NTDs in normal mice (Heid et al., 1992) or in cultured rat embryos (Cockroft, 1991), Fleming and Copp (1998) identified a mouse model of NTD, namely, homozygous Splotch (Pax3) mouse embryos, in which exogenous FA and thymidine prevent NTDs in culture. This observation suggested that the disturbance of DNA synthesis was involved in the pathogenesis of NTDs.

Our observation may explain the vulnerability of embryonic brain to FA deficiency. Craciunescu et al. (2004) reported that FA deficiency decreased progenitor cell proliferation and increased apoptosis in the fetal mouse brain (Craciunescu et al., 2004). In this study, we showed that the activity of de novo DNA synthesis is necessary for primary cultured neural stem cells to proliferate with multipotency. Glial cells can proliferate under the activation of either de novo or salvage DNA synthesis pathway whereas neuronal cells cannot be generated under the activation of salvage pathway alone. Neural tube defect can be prevented by administration of FA during the periconceptual period, which may result from activation of de novo DNA synthesis and differentiation to neurons from neural stem cells. Further studies are necessary to elucidate a role of de novo DNA synthesis pathway in differentiation from neural stem cells into neurons in both embryonic and adult central nervous system.

4. Experimental procedures

4.1. *Neurosphere culture*

Neurosphere cultures were prepared as described previously (Reynolds and Weiss, 1996). In brief, striata were removed from E12.5, E14.5, and E16.5 C57BL/6 mice (Japan SLC, Hamamatsu, Japan) embryos and were mechanically dissociated. In place of the complete D-MEM/F-12 medium (Invitrogen, San Diego, CA), which contains 6 μM FA, 1.5 μM Thy, and 1.5 μM hypoxanthine, the cells were cultured in a custom-prepared deficient D-MEM/F-12 medium lacking FA, Thy, and hypoxanthine in order to stress the availability of precursors for both the de novo pathway (folate derivatives) and salvage pathway (Thy, hypoxanthine) of DNA synthesis. The cells were resuspended in the deficient D-MEM/F-12 medium supplemented with N-2 supplement (Invitrogen) (progesterone, 20 nM; apo-transferrine, 100 μM; sodium selenite, 30 nM; insulin, 25 μg/ml), 20 ng/ml human recombinant (hr-) basic FGF-2 (R&D Systems, Minneapolis, MN), 20 ng/ml hr-EGF (Upstate Biotechnology, Lake Placid, NY), and various concentrations of FA and dNS as described. FA was purchased from Takeda Pharmaceutical Co. Ltd. (Tokyo, Japan) and prepared as a 15 mg/ml stock solution before it was added to the culture at a final concentration of 1.0–400 μM. 2′-deoxyadenosine (dAdo), 2′-deoxycytidine (dCyd), 2′-deoxyguanosine (dGuo), Thy, azathioprine (AZP), and methotrexate (MTX) were purchased from Sigma (St. Louis, MO) and prepared as a 20 mM stock solution in water. Viable single cells at a density of 1.0×10^5 cells/ml were seeded into 75-cm^2 tissue culture flasks and incubated at 37 °C in an atmosphere of 5% CO_2 and treated with 20 ng/ml basic fibroblast growth factor (bFGF) every other day. Secondary neurosphere cultures were prepared by mechanical dissociation of 7 days in vitro (DIV) primary neurospheres into single cells and resuspended at a density of 2.0×10^4 cells/ml in a fresh culture medium. For neurosphere counting, viable single cells at a density of 1.0×10^4 cells/ml were seeded into uncoated 96-well microplates. It has been demonstrated previously that culturing cells at this density will result in clonal neurosphere colonies, as form in single-cell cultures, and that neurospheres do not arise as a result of cell aggregation at the cell culture densities used here (Seaberg and van der Kooy, 2002; Tropepe et al., 2000). To assess their differentiation potential, 7-DIV spheres were plated onto poly-L-ornithine-coated chamber slides (Nunc, Naperville, IL) in D-MEM/F-12 supplemented with N-2 supplement and 10% fetal bovine serum (differentiation condition) and cultured for 4 DIV before fixation for immunocytochemistry. For neuron counting, 7 DIV spheres were mechanically dissociated, and viable cells were resuspended at a density of 5.0×10^4 cells/ml and plated onto the precoated chamber slides under the differentiation condition. Cell numbers and viability were assessed by trypan blue dye exclusion by using a hemocytometer.

Fig. 6 – Inhibitors of de novo DNA synthesis decrease tubulin β III-immunopositive neurons in the neurosphere culture. (A) Experimental protocol. Neurospheres were cultured under the FA+/dNS–, FA–/dNS+, and FA+/dNS+ conditions supplemented with AZP or MTX for 7 DIV. (B and C) Dose–response curves of sphere formation, cultured for 7 DIV under each condition supplemented with AZP (B) and MTX (C). Among the three conditions, the FA+/dNS– condition was the most sensitive to the inhibitors. Graphs show mean ± SEM number of spheres per 1×10^4 cells. (D) Experimental protocol. Spheres formed under the conditions, as described above, were placed under the common differentiation condition. (E) Quantitative analysis of the effects of de novo inhibitors. Graph shows mean ± SEM percentage of tubulin β III-immunopositive neurons of the total number of cells per field derived from the spheres under the FA+/dNS+ condition or under the FA+/dNS+ condition with inhibitors. **Significant difference compared with the FA+/dNS+ condition ($P < 0.01$). (F–I) Double immunocytochemistry for neurons (tubulin β III, red) and astrocytes (GFAP, green). Representative fields derived from the spheres under the FA+/dNS+ conditions (F), FA–/dNS+ (G), FA+/dNS+ with 1 μM AZP (H), and FA+/dNS+ with 0.1 μM MTX (I) conditions are shown. White arrowheads indicate tubulin β III-positive neurons. Scar bars: F–I, 50 μM.

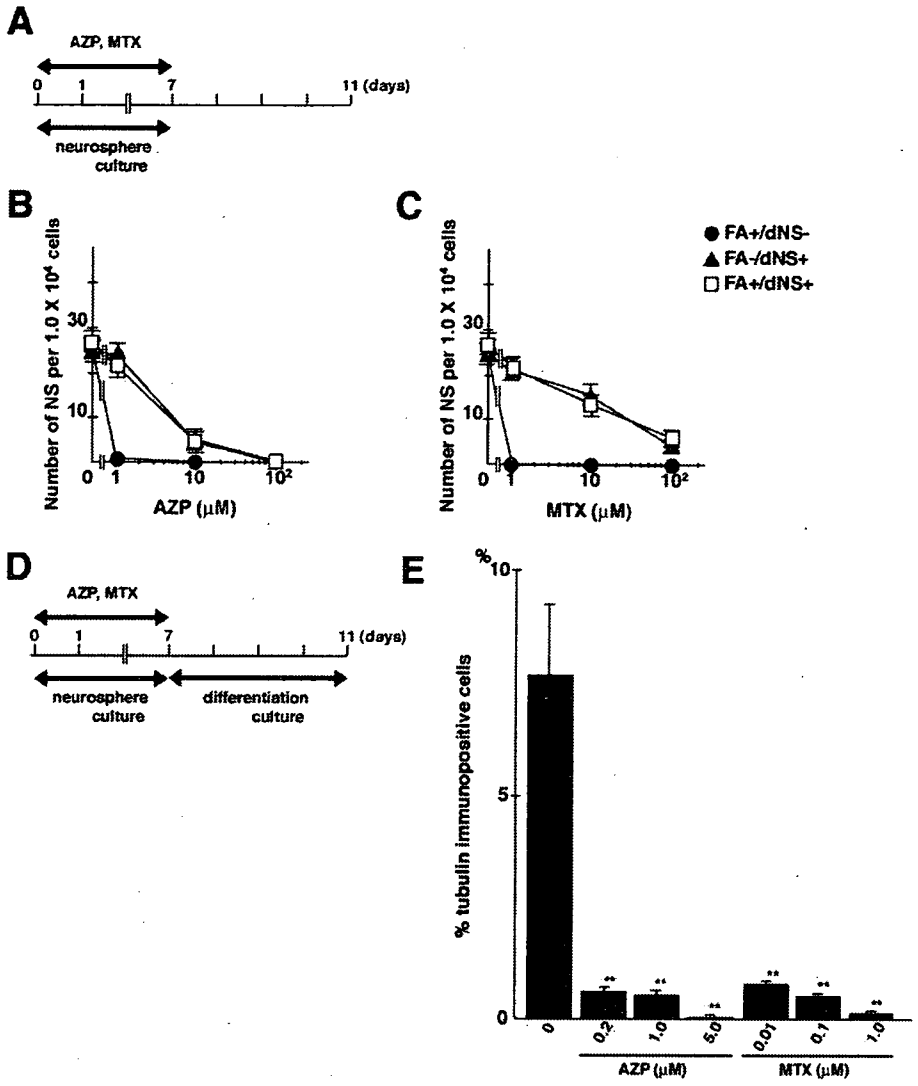
A
AZP, MTX
0 1 7 11 (days)
neurosphere culture
B
Number of NS per 1.0 X 10⁴ cells
30
10
0 1 10 10²
AZP (μM)
C
FA+/dNS-
FA-/dNS+
FA+/dNS+
Number of NS per 1.0 X 10⁴ cells
30
10
0 1 10 10²
MTX (μM)
D
AZP, MTX
0 1 7 11 (days)
neurosphere culture
differentiation culture
E
% tubulin immunopositive cells
%10
5
0
0 0.2 1.0 5.0 0.01 0.1 1.0
AZP (μM)
MTX (μM)

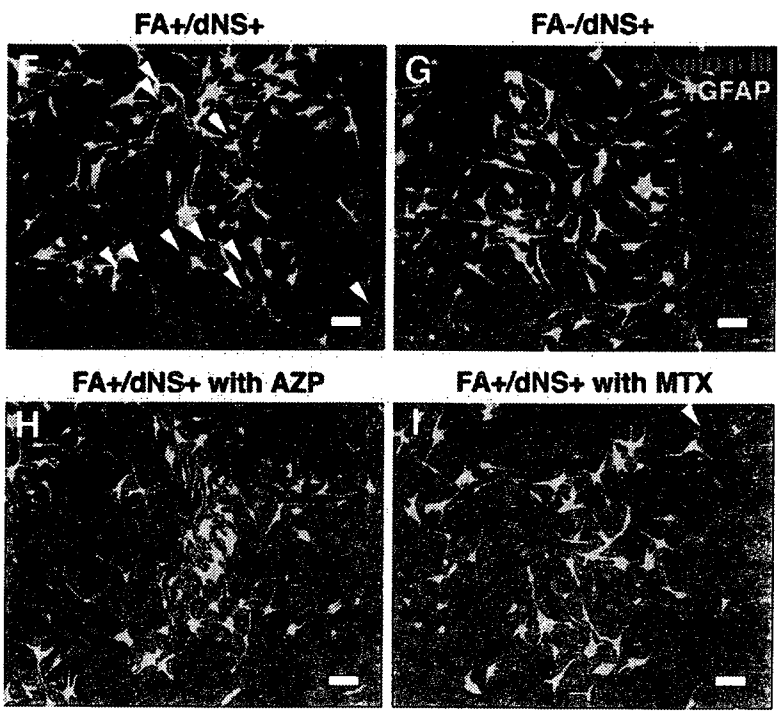
FA+/dNS+
FA-/dNS+
F
G
GFAP
FA+/dNS+ with AZP
FA+/dNS+ with MTX
H
I

4.2. *Immunocytochemistry*

Indirect immunocytochemistry was carried out either immediately after plating (for neurosphere staining) or after 4 DIV (for triple-labeling and for neuronal counting). The cells plated on the precoated chamber slides were fixed in 4% paraformaldehyde for 30 min, followed by permeabilization with 0.3% Triton X-100 for 5 min, and stained by immunofluorescence with the following primary antibodies: mouse anti-tubulin β III (1:200; Chemicon, Temecula, CA), mouse anti-MAP2 (1:500; Chemicon), mouse anti-nestin (1:200; Chemicon), rabbit anti-GFAP (1:400; Dako, Carpinteria, CA), and mouse anti-O4 (1:20, Chemicon). Primary antibodies were visualized with Cy3- (red), AMCA- (blue), and FITC- (green) conjugated secondary antibodies (Jackson Immuno-Research, West Grove, PA). 4′,6-Diamidino-2-phenylindole (DAPI) was used as a fluorescent nuclear counterstain. Stained cultures were examined and photographed by fluorescence microscopy (Leica, Nussloch, Germany).

4.3. *Statistical analysis*

Statistical analyses were carried out using ANOVA or Student's t test. A P value <0.05 was considered significant.

REFERENCES

Ayusawa, D., Shimizu, K., Koyama, H., Kaneda, S., Takeishi, K., Seno, T., 1986. Cell-cycle-directed regulation of thymidylate synthase messenger RNA in human diploid fibroblasts stimulated to proliferate. J. Mol. Biol. 190, 559–567.

Belgi, G., Friedmann, P.S., 2002. Traditional therapies: glucocorticoids, azathioprine, methotrexate, hydroxyurea. Clin. Exp. Dermatol. 27, 546–554.

Chiasson, B.J., Tropepe, V., Morshead, C.M., van der Kooy, D., 1999. Adult mammalian forebrain ependymal and subependymal cells demonstrate proliferative potential, but only subependymal cells have neural stem cell characteristics. J. Neurosci. 19, 4462–4471.

Chu, E., Callender, M.A., Farrell, M.P., Schmitz, J.C., 2003. Thymidylate synthase inhibitors as anticancer agents: form bench to bedside. Cancer Chemother. Pharmacol. 52, S80–S89.

Cockroft, D.L., 1991. Vitamin deficiencies and neural-tube defects: human and animal studies. Hum. Reprod. 6, 148–157.

Craciunescu, C.N., Brown, E.C., Mar, M.H., Albright, C.D., Nadeau, M.R., Zeisel, S.H., 2004. Folic acid deficiency during late gestation decreases progenitor cell proliferation and increases apoptosis in fetal mouse brain. J. Nutr. 134, 162–166.

Czeizel, A.E., Dudas, I., 1992. Prevention of the first occurrence of neural-tube defects by periconceptional vitamin supplementation. N. Engl. J. Med. 327, 1832–1835.

Daly, L.E., Kirke, P.N., Molloy, A., Weir, D.G., Scott, J.M., 1995. Folate levels and neural tube defects. Implications for prevention. J. Am. Med. Assoc. 27, 1698–1702.

Duan, W., Ladenheim, B., Cutler, R.G., Kruman, I.I., Cadet, J.L., Mattson, M.P., 2002. Dietary folate deficiency and elevated homocysteine levels endanger dopaminergic neurons in models of Parkinson's disease. J. Neurochem. 80, 101–110.

Fleming, A., Copp, A.J., 1998. Embryonic folate metabolism and mouse neural tube defects. Science 280, 2107–2109.

Hatse, S., De Clercq, E., Balzarini, J., 1999. Role of antimetabolites of purine and pyrimidine nucleotide metabolism in tumor cell differentiation. Biochem. Pharmacol. 58, 539–555.

Heid, M.K., Bills, N.D., Hinrichs, S.H., Clifford, A.J., 1992. Folate deficiency alone does not produce neural tube defects in mice. J. Nutr. 122, 888–894.

Hyndman, A.G., Zamenhof, S., 1978. Thymidine phosphorylase, thymidine kinase and thymidylate synthetase activities in cerebral hemispheres of developing chick embryos. J. Neurochem. 31, 577–580.

James, S.J., Basnakian, A.G., Miller, B.J., 1994. In vitro folate deficiency induces deoxynucleotide pool imbalance, apoptosis, and mutagenesis in Chinese hamster ovary cells. Cancer Res. 54, 5075–5080.

Karbownik, M., Brzezianska, E., Zasada, K., Lewinski, A., 2003. Expression of genes for certain enzymes of pyrimidine and purine salvage pathway in peripheral blood leukocytes collected from patients with Graves' or Hashimoto's disease. J. Cell. Biochem. 89, 550–555.

Koury, M.J., Horne, D.W., 1994. Apoptosis mediates thymidine prevents erythroblast destruction in folate deficiency anemia. Proc. Natl. Acad. Sci. U. S. A. 99, 4067–4071.

Koury, M.J., Price, J.O., Hicks, G.G., 2000. Apoptosis in megaloblastic anemia occurs during DNA synthesis by a p53-independent, nucleoside-reversible mechanism. Blood 96, 3249–3255.

Kruman, I.I., Kumaravel, T.S., Lohani, A., Pedersen, W.A., Cutler, R.G., Kruman, Y., Haughey, N., Lee, J., Evans, M., Mattson, M.P., 2002. Folic acid deficiency and homocysteine impair DNA repair in hippocampal neurons and sensitize them to amyloid toxicity in experimental models of Alzheimer's disease. J. Neurosci. 22, 1752–1762.

Laeng, P., Pitts, R.L., Lemire, A.L., Drabik, C.E., Weiner, A., Tang, H., Thyagarajan, R., Mallon, B.S., Altar, C.A., 2004. The mood stabilizer valproic acid stimulate GABA neurogenesis from rat forebrain stem cells. J. Neurochem. 91, 238–251.

Laywell, E.D., Rakic, P., Kukekov, V.G., Holland, E.C., Steindler, D.A., 2000. Identification of a multipotent astrocytic stem cell in the immature and adult mouse brain. Proc. Natl. Acad. Sci. U. S. A. 97, 13883–13888.

Lloyd, M.E., Carr, M., McElhatton, P., Hall, G.M., Hughes, R.A., 1999. The effects of methotrexate on pregnancy, fertility and lactation. QJM 92, 551–563.

Mattson, M.P., Shea, T.B., 2003. Folate and homocysteine metabolism in neural plasticity and neurodegenerative disorders. Trends Neurosci. 26, 137–146.

Murray, R.K., Granner, D.K. (Eds.), 1999. Harper's Biochemistry, 25th edition. Appleton and Lange.

Neary, J.T., Rathbone, M.P., Cattabeni, F., Abbracchio, M.P., Burnstock, G., 1996. Trophic actions of extracellular nucleotides and nucleosides on glial and neuronal cells. Trends Neurosci. 19, 13–18.

Olsen, E.A., 1991. The pharmacology of methotrexate. J. Am. Acad. Dermatol. 25, 306–318.

Palmer, T.D., Markakis, E.A., Willhoite, A.R., Safar, F., Gage, F.H., 1999. Fibroblast growth factor-2 activates a latent neurogenic program in neural stem cells from diverse regions of the adult CNS. J. Neurosci. 19, 8487–8497.

Qian, X., Shen, Q., Goderie, S.K., He, W., Capela, A., Davis, A.A., Temple, S., 2000. Timing of CNS cell generation: a programmed sequence of neuron and glial cell production from isolated murine cortical stem cells. Neuron 28, 69–80.

Reynolds, B.A., Weiss, S., 1996. Clonal and population analyses demonstrate that an EGF-responsive mammalian embryonic CNS precursor is a stem cell. Dev. Biol. 175, 1–13.

Schmid, B.P., 1984. Monitoring of organ formation in rat embryos after in vitro exposure to azathioprine, mercaptopurine, methotrexate or cyclosporin A. Toxicology 31, 9–21.

Seaberg, R.M., van der Kooy, D., 2002. Adult rodent neurogenic regions: the ventricular subependyma contains neural stem cells, but the dentate gyrus contains restricted progenitors. J. Neurosci. 22, 1784–1793.

Sherley, J.L., Kelly, T.J., 1988. Regulation of human thymidine kinase during the cell cycle. J. Biol. Chem. 263, 8350–8358.

Sommer, L., Rao, M., 2002. Neural stem cells and regulation of cell number. Prog. Neurobiol. 66, 1–18.
Suleiman, S.A., Spector, R., 1982. Identification, development, and regional distribution of thymidylate synthetase in adult rabbit brain. J. Neurochem. 38, 392–396.
Sung, S.C., 1971. Thymidine kinase in the developing rat brain. Brain Res. 35, 268–271.
Tropepe, V., Coles, B.L.K., Chiasson, B.J., Horsford, D.J., Elia, A.J., McInnes, R.R., van der Kooy, D., 2000. Retinal stem cells in the adult mammalian eye. Science 287, 2032–2036.

© 2005 Wiley-Liss, Inc.

American Journal of Medical Genetics 140A:1–7 (2006)

Rapid Publication

HRAS Mutation Analysis in Costello Syndrome: Genotype and Phenotype Correlation

Karen W. Gripp,[1]* Angela E. Lin,[2] Deborah L. Stabley,[3] Linda Nicholson,[1] Charles I. Scott Jr.,[1] Daniel Doyle,[4] Yoko Aoki,[5] Yoichi Matsubara,[5] Elaine H. Zackai,[6] Pablo Lapunzina,[7] Antonio Gonzalez-Meneses,[8] Jennifer Holbrook,[3] Cynthia A. Agresta,[3] Iris L. Gonzalez,[3] and Katia Sol-Church[3]

[1]Division of Medical Genetics, A. I. duPont Hospital for Children, Wilmington, Delaware
[2]Genetics and Teratology Unit, MassGeneral Hospital for Children, Boston, Massachusetts
[3]Department of Biomedical Research, Nemours' Childrens Clinic, Wilmington, Delaware
[4]Division of Endocrinology, A. I. duPont Hospital for Children, Wilmington, Delaware
[5]Department of Medical Genetics, Tohoku University School of Medicine, Sendai, Japan
[6]Department of Human Genetics, The Children's Hospital of Philadelphia, Philadelphia, Pennsylvania
[7]Department of Genetics, Hospital Universitario La Paz, Madrid, Spain
[8]Service de Dysmorphology, Hospital Universitario Virgen del Rocio, Sevilla, Spain

Received 5 October 2005; Accepted 20 October 2005

Costello syndrome is a rare condition comprising mental retardation, distinctive facial appearance, cardiovascular abnormalities (typically pulmonic stenosis, hypertrophic cardiomyopathy, and/or atrial tachycardia), tumor predisposition, and skin and musculoskeletal abnormalities. Recently mutations in *HRAS* were identified in 12 Japanese and Italian patients with clinical information available on 7 of the Japanese patients. To expand the molecular delineation of Costello syndrome, we performed mutation analysis in 34 North American and 6 European (total 40) patients with Costello syndrome, and detected missense mutations in *HRAS* in 33 (82.5%) patients. All mutations affected either codon 12 or 13 of the protein product, with G12S occurring in 30 (90.9%) patients of the mutation-positive cases. In two patients, we found a mutation resulting in an alanine substitution in position 12 (G12A), and in one patient, we detected a novel mutation (G13C). Five different *HRAS* mutations have now been reported in Costello syndrome, however genotype–phenotype correlation remains incomplete. © 2005 Wiley-Liss, Inc.

Key words: bladder cancer; gain-of-function; *HRAS*; overgrowth syndrome; rhabdomyosarcoma

INTRODUCTION

Costello syndrome (OMIM #218040) is a rare disorder with a distinctive prenatal phenotype (polyhydramnios, overgrowth, edema), postnatal feeding difficulties and failure to thrive, characteristic facial appearance, abnormalities of the heart, skin and musculoskeletal system, and tumor predisposition [reviewed by Hennekam, 2003; Gripp, 2005; Lin et al., 2005]. The risk of neoplasia (approximately 10–15%) [Gripp et al., 2002] influences clinical care, morbidity, and mortality. While the papillomata, which develop throughout childhood in the peri-oral and/or perianal region are the most common benign tumors, the most common malignancy is rhabdomyosarcoma (RMS), typically with embryonal histologic findings [reviewed by Gripp, 2005]. Less common are neuroblastoma, ganglioneuroblastoma, and transitional cell carcinoma of the bladder [Gripp, 2005].

Costello syndrome shares many phenotypic traits with cardio-facio-cutaneous (CFC) syndrome (OMIM #115150), and in some children it may be difficult if not impossible to be certain about the diagnosis. Although Costello, CFC, and Noonan syndrome (OMIM #163950) all share the familiar cardiac phenotype of pulmonic stenosis and/or hypertrophic cardiomyopathy [summarized in Table VII, Lin et al., 2002], the facial appearance and overall phenotype of Noonan syndrome is much less similar

Grant sponsor: Nemours Biomedical Research; Grant sponsor: NIH; Grant number: 1 P20 RR020173-01.

*Correspondence to: Karen W. Gripp, Division of Medical Genetics, A. I. duPont Hospital for Children, PO Box 269, Wilmington, DE 19899. E-mail: kgripp@nemours.org

DOI 10.1002/ajmg.a.31047

WILEY InterScience® DISCOVER SOMETHING GREAT

to Costello syndrome except in the fetal and neonatal period. Noonan syndrome is caused by missense mutations in *PTPN11*, encoding the tyrosine phosphatase SHP2, in about 50% of patients [Tartaglia et al., 2001]. These *PTPN11* mutations lead to a gain-of-function of SHP2 with enhanced phosphatase activity, resulting in increased activation of the mitogen activated protein kinase (MAPK) pathway. Aoki et al. [2005] hypothesized that the gene mutated in Costello syndrome encodes a molecule that functions upstream or downstream of SHP2 in the signal pathway. They identified the *RAS* genes as potential candidates and subsequently showed that germline mutations in *HRAS* are the underlying cause of Costello syndrome. The mutations identified by Aoki et al. [2005] affect one of two amino acids (position 12 and 13 of the protein) previously found to be mutated in malignant tumors.

To increase our understanding of the molecular definition of Costello syndrome and to provide clinical correlation, we report the results of mutation analysis and phenotypic review in 40 North American and European patients.

MATERIAL AND METHODS

Patients

Patients with Costello syndrome were identified at the 2003 and 2005 International Costello Syndrome Meetings, through the Costello Syndrome Family Network and through physician referral. Patients 1–27 and 29–36 (Table I) were enrolled in a research study approved by the Institutional Review Board of the A. I. duPont Hospital for Children (#2003–006). Clinical information was obtained by self-report by the families who completed a standardized data collection form which was updated every 2 years, when possible, and supplemented by review of medical records and interview of the families. Additional patients (Table I, Patients 28, 37–40) were clinically identified by P.L. and A. G.-M. and studied under an IRB approved protocol (CEIC-HULP-2003-PI-362) at the Hospital Universitario La Paz, Madrid, Spain.

Although a patient may have been diagnosed by a local geneticist or other professional, the diagnosis of Costello syndrome was confirmed independently by K.W.G. and A.E. L. based on diagnostic guidelines [Table 14.1, Lin et al., 2005; Proud et al., 2005]. Emphasis was placed on the characteristic growth pattern (especially severe feeding problems and failure to thrive), developmental delay or mental retardation, skin abnormalities, and distinctive hands, especially ulnar deviation, and ligamentous laxity of the fingers. The characteristic craniofacial appearance (macrocephaly, high forehead, unusually curly hair, hypertelorism, fleshy nasal tip, full lips, wide mouth, full cheeks, and fleshy ear lobes) was the most discriminatory and created the most discussion and doubt in diagnosis when atypical. In this series of well-scrutinized patients, all patients had many of these facial findings. Cardiac hypertrophy included hypertrophic cardiomyopathy (also known as asymmetric septal hypertrophy and idiopathic hypertrophic subaortic stenosis), but excluded mild septal thickening [Lin et al., 2002]. Cardiovascular malformations referred to structural congenital heart defects, and excluded valve prolapse, regurgitation, dysplasia, or thickening.

Laboratory Techniques

DNA was extracted from blood, saliva, or cell lines using standard methods. All DNA represents constitutional samples, no tumor samples were analyzed. In the patients enrolled in the North American protocol, genomic DNA was extracted from buccal cells, blood, or from previously established fibroblast cultures using the PureGene DNA Isolation Kit (Gentra Systems, Minneapolis, MN). Genomic DNA was isolated from saliva samples using the Oragen purification kit. A discrete 575 bp region of the *HRAS* gene containing the first translated exon (Exon 2) and flanking intronic regions was amplified by polymerase chain reaction using these primers: forward-ATTTGGGTGCGTGGTTGA, reverse-CCTCTAGAG-GAAGCAGGAGACA. PCR was performed with 150 ng genomic DNA in a 25 µl reaction containing 1× Qiagen Taq Buffer plus Q solution, 3 mM $MgCl_2$, 500 µM each dNTP, 1 µM of each forward and reverse primers and 0.75 U Taq polymerase (Qiagen, Valencia, CA). Reactions were run on a Stratagene robocycler for 30 cycles (30 sec at 94°C, 30 sec at 60°C, and 1 min at 72°C). Genomic fragments containing the remaining translated exons were amplified in the presence of Q-solution and an annealing temperature of 63°C, using primers previously described [Aoki et al., 2005]. Sequencing was performed in both directions using the ABI BigDye Terminator Cycle Sequencing Ready Reaction kit v 3.1, using a 1/4 dilution of the terminator mix, and analyzed on an ABI3130XL Genetic Analyzer.

The protocol used for the Spanish patients varied regarding the primer sequences and reaction conditions used. Polymerase chain reaction and sequencing were performed following standard protocols [Cheng et al., 1994; Williams and Soper, 1995].

We sequenced the entire coding region in all patients in whom no disease causing mutation was identified. Parental samples were sequenced as available, for the amplicon of interest only.

RESULTS

Table I presents the clinical and molecular characteristics of 40 patients (34 North American,

American Journal of Medical Genetics: DOI 10.1002/ajmg.a

TABLE I. Genotype and Phenotype Analysis in 40 Patients With Costello Syndrome

	Mutation				Growth			Clinical features							Cardiac abnormalities		
Pt#	Nucleotide substitution	Amino acid change	Sex	Age	Ht centile	OFC centile	GH deficiency	Polyhydramnios	FTT	Tone	CNS abnormality	Nystagmus	Ulnar deviation	Papillomata	Tumor	Cardiac hypertrophy	Arrhythmia	CVM
1[a]	34G > A	G12S	F	4	−5 SD	90th	−	+	+	↑	−	+	+	−	−	−	SVT	PS
2	34G > A	G12S	F	10	−5 SD	50–75th	−	+	+	↓	Chiari I syrinx	+	+	−	−	−	−	−
3[b,c]	34G > A	G12S	M	22	−5 SD	90th	−	+	+	↓	−	−	+	+	−	HCM severe concentric	SVT, PACs, PVCs	BAV
4[c]	34G > A	G12S	F	28	−4 SD	>98th	+	+	+	−	−	+	−	+	−	−	−	−
5[b]	34G > A	G12S	F	8	−5 SD	3–10th	−	+	+	↓	−	−	+	+	−	HCM	SVT	ASD
6	34G > A	G12S	M	4	−3 SD	90–97th	−	+	+	↓	−	+	−	−	−	−	SVT	−
7[c]	34G > A	G12S	F	20	10th	75th	↓ Rec'd GH	+	+	↓	−	−	+	+	−	−	+	−
8*	34G > A	G12S	F	2	−4SD	75–90th	−	+	+	↓	−	+	+	−	−	HCM	Tachycardia NOS	−
9	34G > A	G12S	M	5	−4 SD	50–75th	↓ Rec'd GH	+	+	↓	−	−	+	−	−	−	−	−
10[b,c]	34G > A	G12S	F	6	−4 SD	>98th	↓ Rec'd GH	+	+	↓	−	+	+	+	−	LVH concentric	−	PSV, VSD
11[b,f,g]	34G > A	G12S	F	9	−5 SD	>98th	↓ Rec'd GH	+	+	−	VM	↓	↓	↓	RMS	HCM Severe	SVT, EAT	PSV, MS
12[c]	34G > A	G12S	M	35	−4 SD	>98th	−	−	+	↓	−	−	+	+	−	−	−	PSV, ASD
13	34G > A	G12S	F	3	−5 SD	75th	↓	↓	↓	-	Chiari I	−	−	−	−	HCM	Severe sinus tachycardia	−
14	34G > A	G12S	M	7	−5 SD	50–75th	+	+	+	−	+	−	−	−	−	−	−	
15[b]	34G > A	G12S	F	9	−5 SD	50th	−	+	+	↓	HC, VPS, Chiari I	+	+	+	−	−	Tachycardia, Bradycardia	PSV
16	34G > A	G12S	F	17	3 SD	>98th	↓ Rec'd GH	+	+	↓	−	+	+	+	Benign bladder tumor			
17	34G > A	G12S	F	10	1–3rd	90th	↓ Rec'd GH	−	+	↓	−	−	+	+	−	−	−	−
18[f]	34G > A	G12S	M	16	−5 SD	90th	↓ Rec'd GH	↓	↓	-	VM	+	+	−	−	LVH	−	−
19[a,b]	34G > A	G12S	F	10	1–3rd	50–75th	−	+	+	↓	−	−	−	−	−	−	−	−
20	34G > A	G12S	M	3	−5 SD	50–75th	−	+	+	↓	−	−	+	+	−	HCM	SVT	−
21	34G > A	G12S	F	6	−5 SD	50–75th	−	+	+	−	−	−	−	−	−	−	−	−
22	34G > A	G12S	F	13	−4 SD	75–90th	↓ Rec'd GH	+	+	−	−	−	+	+	−	−	LQTS	−
23	34G > A	G12S	M	19	−4 SD	>98th	−	+	+	↓	−	−	+	+	−	HCM	−	−
24	34G > A	G12S	F	6	−5 SD	>98th	−	+	+	−	−	+	+	−	−	HCM Severe	↓ NOS	−
25	34G > A	G12S	M	10	−4 SD	75th	+	+	+	↓	−	−	+	−	−	−	−	−
26[b,h]	34G > A	G12S	M	10	−5 SD	25th	↓ Rec'd GH	+	+	−	Chiari I	−	+	−	−	−	−	PSV
27	34G > A	G12S	F	9	−3 SD	>98th	−	+	+	−	HC, VPS	+	−	−		−	−	−
28[b]	34G > A	G12S	M	8	−4 SD	25–50th	−	+	+	↓	HC	+	+	−	−	IHSS	SVT	PS, ASD
29	34G > A	G12S	M	2	−4 SD	50th	+	+	+	−	−	−	+	−	RMS	↓	EAT	−
30[c,b,i]	34G > A	G12S	F	16	5th	>98th	↓ Rec'd GH	−	+	↓	−	−	+	+	−	+	−	−
31*	35G > C	G12A	M	6	−4 SD	75th	−	+	+	↓	HC, VPS	+	+	+	−	−	Sinus tachycardia, persistent	−
32[c,j]	35G > C	G12A	F	21	−5 SD	75–90th	↓ Rec'd GH	−	+	−	−	−	−	+	Bladder CA	−	−	−
33[b]	37G > T	G13C	M	12	5th	>98th	−	+	+	↓	VM	−	−	−	−	LVH	−	−
Patients with No *HRAS* Mutation:																		
34*,a	None		M	6	−3 SD	50–75th	−	−	+	↓	−	−	+	−	−	−	−	−
35*	None		F	2	−5 SD	10–25th	−	+	+	↓	Increased extra axial fluid	+	+	−	−	HCM	−	PSV
36*	None		M	6	−5 SD	>98th	−	+	+	↓	HC	+	+	−	−	HCM	EAT, PVC, PAC	−
37*,k	None		F	1	−3 SD	10th	−	−	+	↓	−	−	−	−	−	−	−	SVPS
38*,k	None		M	3	−3 SD	10–25th	−	+	+	↓	VM	+	+	−	−	−	−	−
39*,k	None		M	4	−3 SD	NA	−	−	+	↓	Hypoplastic CC, Mega cisterna magna	−	−	−	−	−	−	PS
40*,k	None		F	4	4 SD	50–75th	−	+	−	↓	−	−	−	−	−	+ NOS	SVT	PS

ASD, atrial septal defect; BAV, bicuspid aortic valve; CA, carcinoma; CAR, chaotic atrial rhythm; CC, corpus callosum; CNS, central nervous system; CVM, cardiovascular malformation; EAT, ectopic atrial rhythm; F, female; FTT, failure to thrive; GH, growth hormone; HC, hydrocephalus; HCM, hypertrophic cardiomyopathy; Ht, height; IHSS, idiopathic subaortic stenosis; LQTS, prolongation of QT interval; M, male; MS, mitral stenosis; NA, not available; NOS, not otherwise specified; PSV/SV, pulmonic stenosis (valvar, supravalvar); PAC, premature atrial contraction; Pt, patient; RMS, rhabdomyosarcoma; SVT, supraventricular tachycardia; ↑tone increased (↑), tone decreased (↓); VM, ventriculomegaly; VPS, ventriculo-peritoneal shunt; VSD, ventricular septal defect. Age in years, at time measurements for height and OFC were obtained. Height as percentile, or standard deviation when below 1st centile.

Reported previously.

[a]Gripp et al. [2004].

[b]Lin et al. [2002].

[c]White et al. [2005].

[d]Johnson et al. [1998].

[e]Lin et al. [2004].

[f]Dearlove and Harper [1997].

[g]Kerr et al. [1998].

[h]Stein et al. [2004].

[i]Legault and Gagnon [2001].

[j]Gripp et al. [2000].

[k]Spanish patients.

*Indicates overall appearance which was not classic or atypical for Costello syndrome.

6 European) with Costello syndrome. There were 22 females (55%). Ages ranged from 2 to 35 years.

We identified heterozygous *HRAS* mutations in 33 of 40 (82.5%) patients. All mutations occurred de novo, since none of the 19 sets of analyzed parents carried the sequence change. The *HRAS* mutations were identified in different cell types in two patients (Table I, Patient 14: buccal cells and lymphocytes; Patient 18: fibroblasts and lymphocytes) for which different tissues were available, thus indicating that these mutations occurred in the parental germline. Most (30 of 33, 90.9%) of the mutations are 34G > A nucleotide transitions resulting in the substitution of a serine for the glycine in position 12 (G12S). We identified two additional patients with a 35G > C transversion resulting in an alanine substitution in position 12 (G12A). A 37G > T mutation seen in one patient causing a cysteine substitution of amino acid 13 (G13C) has not previously been reported in Costello syndrome (Table II). Table I lists the presumed disease causing nucleotide changes. Several novel single nucleotide polymorphisms (SNPs) were identified in mutation-positive and -negative patients (data not shown). These SNPs were also present in parents and control DNAs isolated from unrelated volunteers and do not appear related to Costello syndrome.

Table III presents a comparison of the clinical characteristics between patients with and without mutations, and between the different mutations.

DISCUSSION

Our results confirm that germline *HRAS* mutations cause Costello syndrome in most patients [Aoki et al., 2005]. All mutations occurred de novo among those triads tested (slightly over half). The patients' missense mutations result in amino acid substitutions of a glycine residue in position 12 or 13 of the protein product. These particular amino acids are located at the GTP binding site and mutations at these sites have previously been shown to cause constitutive activation of HRAS, in turn causing increased activation of downstream effectors in signaling pathways controlling cell proliferation and differentiation [Oliva et al., 2004].

Based on a total of 45 (12 Aoki et al., 2005; 33 in this study) patients with mutations, mutations affecting HRAS amino acids 12 and 13 seem to define a mutational hotspot for Costello syndrome. The phosphate (PO_4) box of the HRAS GTP binding domain encoded by amino acid 10–15 in Exon 2 includes several 5′-CG-3′ (CpG) sites, which could account for this mutational hotspot. When these CpGs are methylated, they become vulnerable to mutations affecting not only the cytosines of either DNA strand, but also the neighboring guanines [Pfeifer, 2000]. Spontaneous mutations can occur at these sites, especially C → T or G → A transitions, with the G → A mutation resulting in the G12S change seen in 30 Costello patients reported here, and 7 previously reported (Table II).

In contrast, nearly 80% of codon 12 mutations seen in tumors [Sanger Institute Catalogue of Somatic Mutations in Cancer, 2005], involve a G → T transversion resulting in amino acid changes G12V or G12C (Table II). The frequency of these mutations is increased in response to mutagens acting on methylated CpG and are very common in many tumor tissues, indicating a high oncogenic potential resulting from the constitutive activation of the protein product. As pointed out by Aoki et al. [2005], the *HRAS* mutation spectrum seen in Costello syndrome differs both qualitatively and quantitatively from the mutation spectrum seen in tumors. The lack of mutations affecting codons other than those in malignancies suggests that there are a limited number of codons in which missense mutations can lead to constitutive activation of the protein product.

Heterozygous missense mutations causing constitutive activation of the protein product often occur in the paternal germline, as suggested by Penrose [1955] who proposed that mitotic replications errors accumulate in male germ cells. Supporting this hypothesis are the findings in Apert syndrome, achondroplasia and Muenke syndrome, due to missense mutations in *FGFR2* and *FGFR3*, respectively, with exclusive paternal origin of new mutations resulting in constitutive activation or increased ligand binding of the protein product [Moloney et al., 1996; Rannan-Eliya et al., 2004]. The paternal age effect observed in Costello syndrome [Lurie, 1994], in combination with

TABLE II. *HRAS* Mutations in Patients With Costello Syndrome and in Tumor Samples

Amino acid change	Nucleotide substitution	Aoki et al. [2005]	This report	Total (%)	Frequency in tumors[a]
G12S	34G → A	7	30	37 (82.2 %)	6.5%
G12A	35G → C	2	2	4 (8.8 %)	0.4%
G13D	38G → A	2	—	2 (4.4 %)	4.4%
G12V[b]	35GC → TT; 35G → T	1	—	1 (2.2%)	44.2%
G13C	37G → T	—	1	1 (2.2%)	0.6%

[a]Frequency in tumors was calculated based on 477 *HRAS* missense mutation positive tumor samples on the Sanger Institute Catalogue of Somatic Mutations in Cancer [2005]. Percentages in the tumors do not add up to 100 because only the amino acid changes seen in Costello syndrome are listed.
[b]The G12V mutations is typically due to a G to T transversion at position 35 in tumors; however, in the Costello patient, a double mutation occurred resulting in the same predicted amino acid change.

TABLE III. Clinical Characteristics and *HRAS* Mutation Status in Patients With Costello Syndrome: Combined Series

Clinical characteristic	No mutation 7 (7,0) pts	*HRAS* mutation present					
		Total 40[a] (33,7) pts	G12S 33 (30,3) pts	G12A 3 (2,1) pts	G13D 2 (0,2) pts	G12V 1 (0,1) pt	G13C 1 (1,0) pt
Failure to thrive	6/7 (86%)	40/40 (100%)	33/33 (100%)	G13D 2 (0,2) pts	G12V 1 (0,1) pt	G13C 1 (1,0) pt	1/1 (100%)
Polyhydramnios	4/7 (57%)	29/33 (87%)	27/30 (90%)	1/2 (50%)	N/A	N/A	1/1 (100%)
Hypotonia	7/7 (100%)	24/33 (72%)	22/30 (73%)	1/2 (50%)	N/A	N/A	1/1 (100%)
Ulnar deviation	4/7 (57%)	25/33 (75%)	24/30 (80%)	1/2 (50%)	N/A	N/A	0/1 (0%)
Any cardiac abnormality	5/7 (71%)	30/40 (75%)	22/33 (66%)	2/3 (66%)	2/2 (100%)	1/1 (100%)	1/1 (100%)
Cardiac hypertrophy	4/7 (43%)	19/40 (47%)	15/33 (45%)	1/3 (33%)	1/2 (50%)	1/1 (100%)	1/1 (100%)
Arrhythmia	2/7 (28%)	17/40 (42%)	15/33 (45%)	1/3 (33%)	1/2 (50%)	0/1 (0%)	0/1 (0%)
CVM	4/7 (57%)	10/40 (25%)	9/33 (27%)	0/3 (0%)	1/2 (50%)	0/1 (0%)	0/1 (0%)
Papillomata	0/7 (0%)	19/40 (47%)	16/33 (48%)	2/3 (66%)	1/2 (50%)	0/1 (0%)	0/1 (0%)
GH deficiency	0/7 (0%)	15/33 (45%)	14/30 (46%)	1/2 (50%)	N/A	N/A	0/1 (0%)
Nystagmus	3/7 (43%)	14/33 (42%)	13/30 (43%)	1/2 (50%)	N/A	N/A	0/1 (0%)
Tumor	0/7 (0%)	6/40 (15%)	4/33 (12%)	2/3 (66%)	0/2 (0%)	0/1 (0%)	0/1 (0%)
CNS abnormality	4/7 (57%)	9/33 (27%)	8/30 (27%)	1/2 (50%)	N/A	N/A	1/1 (100%)

Figures are rounded.

CNS, central nervous system abnormality; CVM, cardiovascular malformation; GH, growth hormone.

[a]Patient total includes the 33 new patients listed on Table I in this report, and the 7 Japanese patients listed on the supplementary Table I (online version) of Aoki et al. [2005]; no information was available on the five Italian patients from that series. Patients are listed as the total, followed in parentheses by the number in the present series and Japanese patients. There was no information on polyhydramnios, growth hormone deficiency, hypotonia, nystagmus, and ulnar deviation was provided by Aoki et al. [2005], and thus, denominators reflect the number of informative patients.

the nature of the missense mutations, suggests a paternal origin of the mutations. In this context, the loss of heterozygosity (LOH) of 11p15.5 in tumor tissue from Costello syndrome cases is of particular interest. Kerr et al. [2003] analyzed five embryonal RMS from Costello syndrome patients and showed loss of heterozygosity for 11p15.5 in all samples, with retention of the paternal allele confirmed in two cases. This finding may be consistent with the monoallelic expression of the mutated allele in the ganglioneuroblastoma described by Aoki et al. [2005]. It remains to be seen if LOH for *HRAS* is a consistent finding in all tumors in Costello syndrome, or if it is typical only for embryonal tumors as reported by Kerr et al. [2003] and Aoki et al. [2005]. While the constitutional *HRAS* mutation in Costello patients represents the first step in tumorigenesis, the second step may vary with LOH in embryonal tumors and mutations in additional genes in bladder cancer and other malignancies of adulthood. Jebar et al. [2005] reviewed *FGFR3* and *RAS* mutations in urothelial cell carcinoma and did not identify LOH, rather they reported mutually exclusive sequence changes in the genes whose protein products share the MAPK pathway as common effector.

The lack of mutations in seven patients led us to review their respective clinical presentation in detail. All patients except Patients 34 and 36 enrolled under the North American study were thought to have the typical facial changes of Costello syndrome. Upon review of facial photographs of the patients enrolled under the Spanish protocol, only Patient 28 had the completely characteristic facial appearance of Costello syndrome, and Patients 37–40 had facial findings consistent with either Costello or CFC syndrome. At this time, we cannot be certain that the lack of an identifiable *HRAS* mutation excludes the diagnosis of Costello syndrome. The possibility that these patients do not have Costello, but possibly CFC syndrome needs to be considered. If this was confirmed, the phenotype of CFC syndrome would include elevated catecholamine metabolite levels and cardiac arrhythmia.

It is noteworthy that we identified *HRAS* mutations in Patients 11, 29, and 30, who each had a malignancy, and Patient 16, who reportedly had a benign bladder tumor. Patient 30 developed a transitional cell carcinoma of the bladder [Gripp et al., 2000], she carries a mutation predicted to result in a G12A amino acid substitution. This mutation is found in less than 1% of malignancies with an *HRAS* mutation (Table II), specifically in one chondrosarcoma and one papillary thyroid carcinoma [Sanger Institute Catalogue of Somatic Mutations in Cancer, 2005]. In contrast, the G12S change present in Patients 11 and 29 with RMS represents the most common mutation in Costello syndrome and occurs in a variety of malignancies including soft tissue and synovial sarcoma and carcinoma of the gastro-intestinal and urinary tract [Sanger Institute Catalogue of Somatic Mutations in Cancer, 2005]. This mutation was seen in a Japanese patient with rhabdomyosarcoma [Aoki et al., 2005]. We identified one novel CS mutation, resulting in a cysteine substitution of amino acid 13 (Table I, Patient 33). This particular mutation is relatively rare in malignancies, but has been identified in three bladder cancer samples [Visvanathan et al., 1988; Levesque et al., 1993]. While it may be tempting to speculate on the oncogenic potential of the different mutations, we need more data to evaluate if the cancer risk varies by mutation.

Most of our patients and those reported by Aoki et al. [2005] share a common mutation (Table II). Rare phenotypic findings in these patients, for example

the long QT syndrome in Patient 22, may be coincidental, or caused by the mutation with a low incidence or in combination with modifying factors. A correlation between the cardiac abnormalities and the specific mutations is also hampered by the fact that we have few patients with mutations other than G12S. Of the three patients with mutations other than G12S, one each had left ventricular hypertrophy and tachycardia. While none had pulmonic stenosis or other structural anomalies, these numbers are too small to draw conclusions. Of note are the cardiac anomalies seen in some of the *HRAS* mutation-negative patients: Three had hypertrophic cardiomyopathy, two showed tachyarrhythmia, and four had pulmonic stenosis. Concerning the short stature seen in almost all Costello patients, Patient 33, the only person reported to date with the G13C mutation, is noteworthy. He is the tallest mutation-positive patient who never received growth hormone, and at age 12 years, he has not developed papillomata. This may suggest that G13C causes a slightly less severe phenotype.

The identification of *HRAS* mutations as the underlying cause for Costello syndrome is very helpful in respect to the ability to confirm a clinical diagnosis of Costello syndrome. Based on the data available today, a *HRAS* missense mutation leading to constitutive activation of the protein, in combination with consistent clinical findings, is likely diagnostic of Costello syndrome. In contrast, we cannot be certain that the lack of such a mutation precludes a diagnosis of Costello syndrome. It is too early to revise recommendations for clinical care based on the mutation status, but we hope to collect additional data in order to achieve this goal. Lastly, one may speculate that the identification of these mutations in Costello syndrome in combination with the knowledge from cancer research on *HRAS* and the MAPK pathway will allow for the use of medications directed at this pathway.

ACKNOWLEDGMENTS

We thank the families, individuals with Costello syndrome, and professionals of the Costello Syndrome support groups around the world, and Lisa Schoyer, president of the Costello Syndrome Family Network. This report was supported by Nemours Biomedical Research and by funds to KSC from NIH grant number 1 P20 RR020173-01 from the National Center for Research Resources.

REFERENCES

Aoki Y, Niihori T, Kawame H, Kurosawa K, Ohashi H, Tanaka Y, Filocamo M, Kato K, Suzuki Y, Kure S, Matsubara Y. 2005. Germline mutations in HRAS proto-oncogene cause Costello syndrome. Nat Genet 37:1038–1040.

Cheng S, Fockler C, Barnes WM, Higuchi R. 1994. Effective amplification of long targets from cloned inserts and human genomic DNA. Proc Natl Acad Sci USA 91:5695–5699.

Dearlove O, Harper N. 1997. Costello syndrome. Paediatr Anaesth 7:476–477.

Gripp KW. 2005. Tumor predisposition in Costello syndrome. Am J Med Genet 137C:72–77.

Gripp KW, Scott CI Jr, Nicholson L, Figueroa TE. 2000. A second case of bladder carcinoma in a patient with Costello syndrome. Am J Med Genet 90:256–259.

Gripp KW, Scott CI Jr, Nicholson L, McDonald-McGinn DM, Ozeran JD, Jones MC, Lin AE, Zackai EH. 2002. Five additional Costello syndrome patients with rhabdomyosarcoma: Proposal for a tumor screening protocol. Am J Med Genet 108: 80–87.

Gripp KW, Kawame H, Viskochil DH, Nicholson L. 2004. Elevated catecholamine metabolites in patients with Costello syndrome. Am J Med Genet 128A:48–51.

Hennekam RCM. 2003. Costello syndrome: An overview. Am J Med Genet 117C:42–48.

Jebar AH, Hurst CD, Tomlinson DC, Johnston C, Taylor CF, Knowles MA. 2005. FGFR3 and Ras gene mutations are mutually exclusive genetic events in urothelial cell carcinoma. Oncogene 24:5218–5225.

Johnson JP, Golabi M, Norton ME, Rosenblatt RM, Feldman GM, Yang SP, Hall BD, Fries MH, Carey JC. 1998. Costello syndrome: Phenotype, natural history, differential diagnosis, and possible cause. J Pediatr 133:441–448.

Kerr B, Eden TOB, Dandamudi R, Shannon N, Quarrell O, Emmerson A, Ladusans E, Gerrard M, Donnai D. 1998. Costello syndrome: Two cases with embryonal rhabdomyosarcoma. J Med Genet 335:1036–1039.

Kerr B, Mucchielli ML, Sigaudy S, Fabre M, Saunier P, Voelckel MA, Howard E, Elles R, Eden TOB, Black GC, Philip N. 2003. Is the locus for Costello syndrome on 11p?. J Med Genet 40:469–471.

Legault L, Gagnon C. 2001. Growth hormone deficiency in Costello syndrome: A possible explanation for the short stature. J Pediatr 138:151–152.

Levesque P, Ramchurren N, Saini K, Joyce A, Libertino J, Summerhayes IC. 1993. Screening of human bladder tumors and urine sediments for the presence of H-ras mutations. Int J Cancer 55:785–790.

Lin AE, Grossfeld PD, Hamilton R, Smoot L, Proud V, Weksberg R, Gripp KW, Wheeler P, Picker J, Irons M, Zackai EH, Scott CI, Nicholson L. 2002. Further delineation of cardiac anomalies in Costello syndrome. Am J Med Genet 111:115–129.

Lin AE, Harding C, Silberbach M. 2004. Hand it to the skin in Costello syndrome. J Pediatr 144:135.

Lin AE, Gripp KG, Kerr BK. 2005. Costello syndrome. In: Cassidy SB, Allanson JE, editors. Management of genetic syndromes. 2nd edition Hoboken: Wiley Liss, pp 151–162.

Lurie IW. 1994. Genetics of the Costello syndrome. Am J Med Genet 52:358–359.

Moloney DM, Slaney SF, Oldridge M, Wall SA, Sahlin P, Stenman G, Wilkie AO. 1996. Exclusive paternal origin of new mutations in Apert syndrome. Nat Genet 13:48–53.

Oliva JL, Zarich N, Martinez N, Jorge R, Castrillo A, Azanedo M, Garcia-Vargas S, Gutierrez-Eisman S, Juarranz A, Bosca L, Gutkind JS, Rojas JM. 2004. The P34G mutation reduces the transforming activity of K-Ras and N-Ras in NIH 3T3 cells but not of H-Ras. J Bio Chem 279:33480–33489.

Penrose LS. 1955. Parental age and mutation. Lancet 2:312–313.

Pfeifer GP. 2000. p53 mutational spectra and the role of methylated CpG sequences. Mutat Res 450:155–166.

Proud VK, Creswick HA, Schoyer L. 2005. Costello syndrome: Developing diagnostic criteria. Proc Greenwood Genet Ctr 24:126A.

Rannan-Eliya SV, Taylor IB, De Heer IM, Van Den Ouweland AM, Wall SA, Wilkie A. 2004. Paternal origin of FGFR3 mutations in Muenke-type craniosynostosis. Hum Genet 115:200–207.

Sanger Institute Catalogue of Somatic Mutations in Cancer. 2005. Distribution of somatic mutations in HRAS. www.sanger.ac.uk

Stein RI, Legault L, Daneman D, Weksberg R, Hamilton J. 2004. Growth hormone deficiency in Costello syndrome. Am J Med Genet Part A 129A:166–170.

Tartaglia M, Mehler EL, Goldberg R, Zampino G, Brunner HG, Kremer H, van der Burgt I, Crosby AH, Ion A, Jeffery S, Kalidas K, Patton MA, Kucherlapati RS, Gelb BD. 2001. Mutations in PTPN11, encoding the protein tyrosine phosphatase SHP-2, cause Noonan syndrome. Nat Genet 29:465–468.

Visvanathan KV, Pocock RD, Summerhayes IC. 1988. Preferential and novel activation of H-ras in human bladder carcinomas. Oncogene Res 3:77–86.

White SM, Graham JM, Kerr B, Gripp K, Weksberg R, Cytrynbaum C, Reeder JL, Stewart FJ, Edwards M, Wilson M, Bankier A. 2005. The adult phenotype in Costello syndrome. Am J Med Genet 136A:128–135.

Williams DC, Soper SA. 1995. Ultrasensitive near-IR fluorescence detection for capillary gel electrophoresis and DNA sequencing applications. Anal Chem 67:3427–3432.

Direct Correlation Between Ischemic Injury and Extracellular Glycine Concentration in Mice With Genetically Altered Activities of the Glycine Cleavage Multienzyme System

Masaya Oda, MD; Shigeo Kure, MD; Taku Sugawara, MD; Suguru Yamaguchi, MD; Kanako Kojima, MD; Toshikatsu Shinka, MD; Kenichi Sato, MD; Ayumi Narisawa, MD; Yoko Aoki, MD; Yoichi Matsubara, MD; Tomoya Omae, MD; Kazuo Mizoi, MD; Hiroyuki Kinouchi, MD

Background and Purpose—Ischemia elicits the rapid release of various amino acid neurotransmitters. A glutamate surge activates *N*-methyl-D-aspartate (NMDA) glutamate receptors, triggering deleterious processes in neurons. Although glycine is a coagonist of the NMDA receptor, the effect of extracellular glycine concentration on ischemic injury remains controversial. To approach this issue, we examined ischemic injury in mice with genetically altered activities of the glycine cleavage multienzyme system (GCS), which plays a fundamental role in maintaining extracellular glycine concentration.

Methods—A mouse line with increased GCS activity (340% of C57BL/6 control mice) was generated by transgenic expression of glycine decarboxylase, a key GCS component (high-GCS mice). Another mouse line with reduced GCS activity (29% of controls) was established by transgenic expression of a dominant-negative mutant of glycine decarboxylase (low-GCS mice). We examined neuronal injury after transient occlusion of the middle cerebral artery in these mice by measuring extracellular amino acid concentrations in microdialysates.

Results—High-GCS and low-GCS mice had significantly lower and higher basal concentrations of extracellular glycine than did controls, respectively. In low-GCS mice, the extracellular glycine concentration reached 2-fold of control levels during ischemia, and infarct volume was significantly increased by 69% with respect to controls. In contrast, high-GCS mice had a significantly smaller infarct volume (by 21%). No significant difference was observed in extracellular glutamate concentrations throughout the experiments. An antagonist for the NMDA glycine site, SM-31900, attenuated infarct size, suggesting that glycine operated via the NMDA receptor.

Conclusions—There is a direct correlation between ischemic injury and extracellular glycine concentration maintained by the GCS. (***Stroke.* 2007;38:2157-2164.**)

Key Words: animal models ■ glutamate ■ glycine ■ neuroprotection ■ NMDA glutamate receptor ■ reperfusion ■ transgenic mice

An abnormal increase in extracellular glycine concentration, together with a rapid elevation of glutamate, is consistently elicited by ischemia.[1] The elevation of glutamate leads to uncontrolled activation of *N*-methyl-D-aspartate (NMDA) receptors and intracellular penetration of calcium, which is followed by production of free radicals, mitochondrial dysfunction, DNA injury, and deleterious processes that finally lead to the demise of surrounding neurons.[2] Activation of NMDA receptors is therefore considered a key process in the development of ischemic injury. Glycine is an inhibitory neurotransmitter in the brain stem and spinal cord,[3] and it also plays a critical role as a modulator of NMDA receptors.[2-4] The role of glycine in stroke remains controversial. In acutely prepared hippocampal slices, excitotoxicity and subsequent neuronal cell death could be induced by addition of high concentrations of glycine.[5] These toxic effects were, however, observed only when a millimolar concentration of glycine was applied, whereas the peak level of extracellular glycine during ischemia was in the micromolar range.[6] In contrast, high extracellular glycine failed to potentiate NMDA-evoked depolarization in vivo.[7] Glycine protected neurons from hypoxia-induced toxicity in cortical neuron cultures.[8] Recently, several antagonists at the glycine site of the NMDA receptor have been developed, and their neuro-

Received November 6, 2006; accepted January 22, 2007.

From the Division of Neurosurgery (M.O., T. Sugawara, S.M., T.O., K.M., H.K.), Department of Neuro and Locomotor Science, Akita University School of Medicine, Akita; the Department of Medical Genetics (S.K., K.K., T. Shinka, K.S., A.N., Y.A., Y.M.), Tohoku University School of Medicine, Sendai; and the Department of Neurosurgery (H.K.), Faculty of Medicine, University of Yamanashi, Tamaho, Yamanashi Japan.

Correspondence to Shigeo Kure, MD, Department of Medical Genetics, Tohoku University School of Medicine, 1-1 Seiryomachi, Aobaku, 980-8574, Japan. E-mail skure@mail.tains.tohoku.ac.jp

© 2007 American Heart Association, Inc.

Stroke is available at http://www.strokeaha.org

DOI: 10.1161/STROKEAHA.106.477026

protective effect was reported in experimental stroke.[9] Based on these in vitro effects of glycine and the in vivo effects of antagonists for the NMDA receptor glycine site, it has been repeatedly suggested that glycine may contribute to the development of ischemic injury.[10] To the best of our knowledge, however, no direct evidence has been provided for the in vivo effect of extracellular glycine concentrations on ischemic injury. It is probably because there is no set of experimental animals that have distinct concentrations of extracellular glycine.

Glycine is released from the presynaptic membrane to the synaptic cleft and then either transferred into presynaptic neurons or transported into astrocytes through glycine-specific transporters.[11] In astrocytes, the glycine cleavage system (GCS) degrades glycine efficiently and generates the concentration gradient between the cytosol and extracellular space,[11–13] which enables glycine transporters to transfer glycine from the synaptic cleft into the astrocyte. The distribution of the GCS is inversely related to local glycine levels in the brain,[12] indicating its importance in determination of basal glycine concentrations. The GCS is a mitochondrial enzyme complex with 4 individual components: glycine decarboxylase (GLDC), aminomethyl transferase, aminomethyl carrier protein, and lipoamide dehydrogenase.[14] GLDC is a homodimeric enzyme of ≈200 kDa. An inherited deficiency of either GLDC or aminomethyl transferase causes an inborn error of metabolism, glycine encephalopathy (GE), also called nonketotic hyperglycinemia.[15] GE is characterized by neonatal coma and convulsions associated with the accumulation of large amounts of glycine in cerebrospinal fluid, providing further evidence that the GCS plays a fundamental role in maintaining extracellular glycine concentrations in the central nervous system.

To clarify the role of extracellular glycine in brain ischemia, we examined neuronal injury after transient occlusion of the middle cerebral artery (MCA) in mice with altered GCS activities by monitoring extracellular amino acid concentrations. Mice with altered GCS activities were generated by transgenic expression of normal GLDC or a dominant-negative mutant of GLDC, which was previously found in a family with GE[16] and characterized in this study. These approaches have enabled us for the first time to elucidate a direct correlation between extracellular glycine concentrations and ischemic injury.

Materials and Methods

Expression Analysis of GLDC cDNA in COS7 Cells

We previously identified a 3-base deletion, c.2266 to 2268delTTC, in the *GLDC* gene in a GE family, which resulted in the deletion of 1 phenylalanine residue at amino acid position 756, delF756.[16] The mother was a heterozygous carrier of the 3-base deletion and had a serum glycine level 1.8-hold higher than normal, which is considered the upper limit of the normal range. This observation prompted us to test whether the delF756 mutation had a dominant-negative effect. A 3.7-kb DNA fragment encoding human GLDC cDNA was subcloned into a pCAG vector (P-wild) for expression analysis (Figure 1A). The pCAG vector was kindly provided by Prof Jun-ichi Miyazaki of Osaka University (Osaka, Japan).[17] Mutant GLDC cDNA with the delF756 mutation was also subcloned into pCAG (P-delF756). The pCAG vector containing β-galactosidase cDNA was prepared as a negative control. Plasmid DNAs of the pCAG vector, P-wild, P-delF756, and β-galactosidase were purified with a plasmid purification midi kit (Qiagen GmbH, Hilden, Germany). Preparation of COS7 cells, transfection with lipofectamine (Invitrogen Corp, Carlsbad, Calif), cell harvest, and assay of GLDC enzymatic activity were performed as described.[16]

Generation of Transgenic Mouse Lines

P-wild and P-delF756 plasmids were digested with *Sal*I, and a 5.4-kb DNA fragment was recovered (Figure 1A). After purification of the DNA fragments, they were injected into fertilized eggs of BDF1 mice for generation of transgenic mice. Genomic DNA was purified from mouse tails with use of a DNeasy tissue kit (Qiagen), and a 201-bp DNA fragment of the CAG promoter region was amplified by polymerase chain reaction with a pair of primers, RBGP-1 and -2, for identification of the transgene. Nucleotide sequences of the primers were as follows: for RBGP-1, 5′-GCCCCTTGAGCATCTG ACTTCTGG-3′ and for RBGP-2, 5′-GACCTCTTTATAGCCACCTT TG-3′. We mated the founder mice with C57BL/6 strain mice to obtain F_1 mice and screened for cerebral glycine concentration. Transgenic mice of 2 selected lines, high-GCS and low-GCS mice, were backcrossed with C57BL/6 mice 10 times and used for the following studies.

Enzymatic Analysis of GLDC and GCS Activity

GLDC enzymatic activity was determined by an exchange reaction between CO_2 and glycine with $NaH[^{14}C]O_3$ as described.[16] GCS activity was measured by a decarboxylation reaction with [1-^{14}C]glycine as described.[13]

Regional Cerebral Blood Flow Measurement

Regional cerebral blood flow was measured by the laser-Doppler flowmeter method with a Laserflo BPM2 (Vasamedics, St. Paul, Minn). The flowprobe (0.5-mm diameter) was placed on the cranial bone above the MCA territory (0.5 mm posterior and 4 mm lateral from the bregma) and away from large surface vessels. Steady-state baseline values were recorded before MCA occlusion, and blood flow data were then expressed as percentages of preocclusion baseline. No significant difference in the percent change in cerebral blood flow values was detected during and after ischemia (supplemental Figure I, available online at http://stroke.ahajournals.org).

Induction of Focal Cerebral Ischemia

Males of high-GCS, low-GCS, and control C57BL/6 mouse lines weighing 25 to 30 g were used for the ischemia study. Anesthesia was induced with 2% halothane in a closed chamber and maintained with 1.0% to 1.5% halothane in 30% O_2 and 70% N_2O delivered via facemask. Rectal temperature was monitored and maintained at 37±0.5°C with a thermal blanket throughout the surgical procedure. Focal cerebral ischemia was induced by MCA occlusion by the intraluminal suture technique.[18] A 5–0 nylon monofilament suture with a round tip was inserted into the internal carotid artery 11±0.5 mm from the bifurcation of the common carotid artery until the laser-Doppler flowmeter signal abruptly dropped. After 60 minutes of MCA occlusion, the nylon suture was removed and blood flow restoration was confirmed by the laser-Doppler flowmeter signal. Mice in which the laser-Doppler flowmeter signal during ischemia exceeded 10% of the preischemic signal were excluded from this study. All experiments and surgical procedures were approved by the Akita University Animal Care and Use Committee.

In Vivo Microdialysis

Twenty-four hours before MCA occlusion, vertical microdialysis probes (0.22-mm outer diameter, 2-mm membrane length; Eicom Corp, Tokyo, Japan) were stereotaxically implanted in the left striatum of mice under anesthesia. The probe was coordinately implanted at 0.6 mm anterior and 2.0 mm lateral to the bregma and 2 mm ventral from the brain surface, according to the 1997 atlas of Franklin and Paxinos. The external portions of the probes were fixed to the skull with dental cement. Throughout ischemia, dialysis probes were perfused with Ringer's solution (147 mmol/L NaCl,

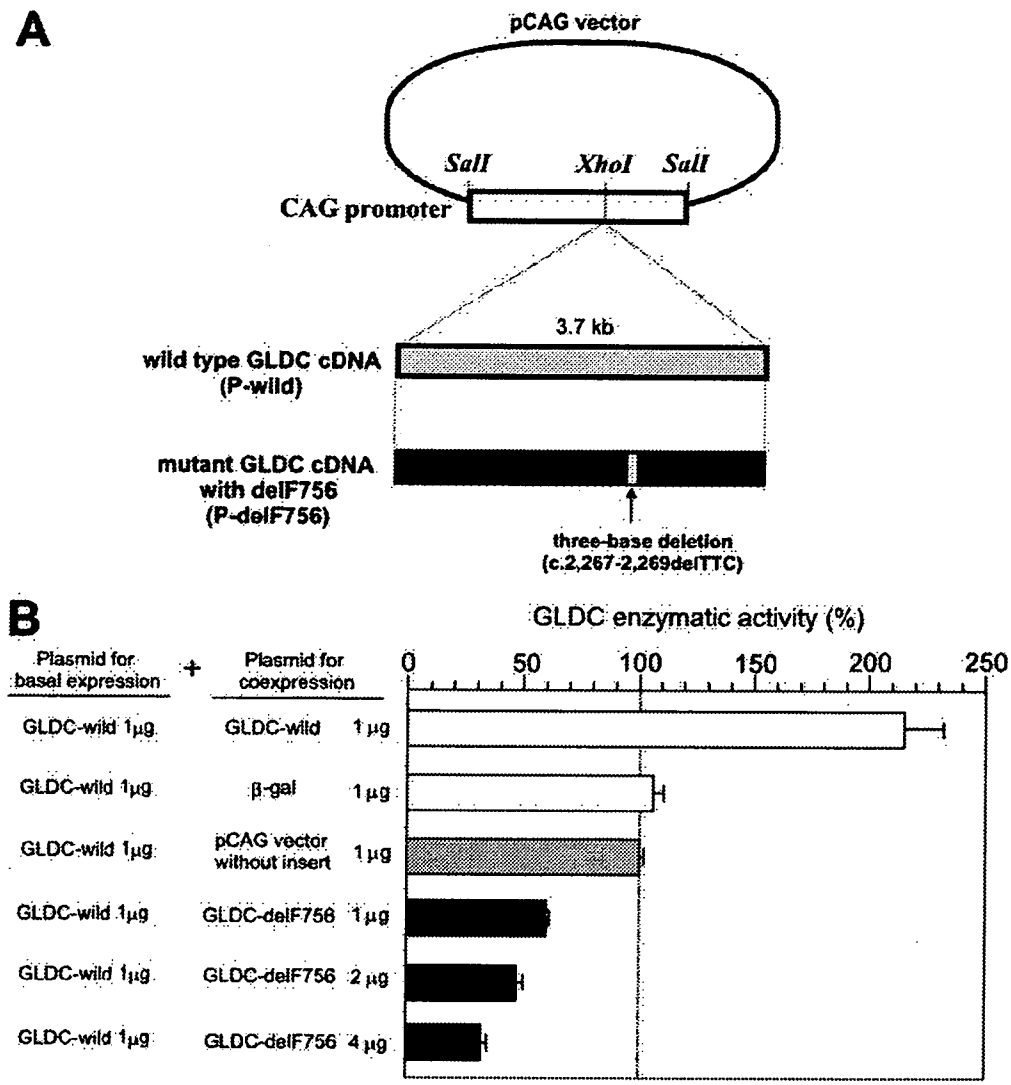

Figure 1. Expression analysis of GLDC cDNA in COS7 cells. A, Construct of expression vectors. Normal human GLDC cDNA (≈3.7 kb) was inserted into the *XhoI* site of the pCAG plasmid (P-wild). A mutant GLDC cDNA with the 3-base deletion, c.2266 to 2268delTTC, was similarly inserted into the pCAG plasmid (P-delF756). B, Coexpression study of P-wild and P-delF756 expression plasmids in COS7 cells. One microgram of P-wild plasmid, together with various other plasmids, was transfected into COS7 cells. The GLDC activity of COS7 cells transfected with 1 μg P-wild plasmid and 1 μg pCAG plasmid was defined as 100%, and relative GLDC activity (%) is shown. Note that less GLDC activity was observed when more P-delF756 plasmid was transfected with the fixed amount of P-wild plasmid.

2.3 mmol/L $CaCl_2$, 4.0 mmol/L KCl; pH 7.0) at a rate of 2 μL/min. The microdialysate (20 μL) was collected every 10 minutes. After a stabilization period of 1 hour, the samples were collected from 1 hour before MCA occlusion to 2 hours after MCA occlusion. Amino acid concentrations in the samples were measured by high-performance liquid chromatography (Eicom Corp).

Administration of SM-31900

An inhibitor of the glycine binding site of the NMDA receptor, SM-31900 (Sunitomo Pharmaceuticals Co Ltd, Osaka, Japan), was dissolved in physiological saline, which was then adjusted to pH 8.5.[19] The animals subjected to MCA occlusion were randomly assigned to vehicle or SM-31900 treatment groups. Vehicle or SM-31900 (10 mg/kg IV) was administered twice at 30 and 10 minutes before MCA occlusion.

Measurement of Infarct Size and Infarct Volume

Twenty-four hours after MCA occlusion, the mice were deeply anesthetized and decapitated. The brain was removed and sectioned coronally into four 2-mm slices with a mouse brain matrix (Harvard Apparatus, Cambridge, Mass). The slices then were placed in 2% 2,3,5-triphenyltetrazolium chloride solution at 37°C for 10 minutes and fixed in a 10% buffered formalin solution. The infarct area, stained white, was measured with NIH Image analysis software, and infarct volume was calculated by summing the infarct volumes of sequential 2-mm-thick sections.[20] Infarct volume was measured in different groups of animals from those used for microdialysis studies because infarct volume cannot be evaluated after probe insertion for microdialysis.

Statistics

All data were expressed as mean±SD. The statistical differences in regional cerebral blood flow and amino acid concentrations among and within the mouse groups were analyzed by a 1-way ANOVA and Dunnetts's test for multiple comparisons. Significance was accepted with $P<0.05$.

Results

Identification of Dominant-Negative GLDC

When 1 μg of plasmid with normal human GLDC cDNA (P-wild) was expressed in COS7 cells, the specific GLDC

activity was 9.8±0.8 nmol of glycine formed per milligram protein per hour, which was defined as 100% GLDC activity (Figure 1B). Expression of 2 μg of P-wild plasmid resulted in 215.8±19% GLDC activity. Negligible GLDC activity was detected in transfection of 1 μg of P-delF756 plasmid.[16] GLDC activity was reduced to 62.1±0.3%, 47.0±1.9%, and 32.0±1.6% in cotransfection with 1, 2, and 4 μg P-delF756 plasmid together with 1 μg P-wild plasmid, respectively (Figure 1B). No reduction in GLDC activity was observed when 1 μg β-galactosidase plasmid was cotransfected. Because GLDC activity was inhibited in response to amounts of P-delF756, we concluded that the delF756 mutation had a dominant-negative effect.

Generation and Biochemical Characterization of the High-GCS Mouse Line

Normal GLDC cDNA and mutant GLDC cDNA with the delF756 mutation were subjected to transgenic expression in mice under control of the CAG promoter (Figure 1A). A *SalI/SalI* fragment (5.4 kb) of P-wild plasmid containing normal human GLDC cDNA was injected into 50 fertilized eggs. A total of 13 mice were born. One of them turned out to carry the transgene. It grew normally and was fertile to establish a transgenic mouse line. Mice of this line had significantly lower cerebral glycine concentrations (0.71±0.06 μmol/g wet tissue) than did wild-type C57BL/6 mice (0.90±0.05) as shown in Figure 2A. The enzymatic activity of the GCS was determined by a glycine decarboxylation reaction in tissue samples of mouse cerebrum. GCS activity was 0.48±0.14 nmol of CO_2 formed per milligram protein per hour, which was 340% of that of wild-type C57BL/6 mice (0.14±0.03). This transgenic mouse line was designated high GCS.

Generation and Biochemical Characterization of the Low-GCS Mouse Line

A *SalI/SalI* fragment (5.4 kb) of the P-delF756 plasmid containing mutant human GLDC cDNA (Figure 1A) was injected into 225 fertilized eggs, and 72 mice were born. The transgene was identified in 15 of 72 mice. By 3 months of age, 5 of 15 founder mice had died of unknown causes. We observed that 1 of those 5 mice exhibited shivering and loss of body weight at 3 month of age. Measurement of amino acid contents in the brain sample from that mouse showed a marked increase in glycine content, 3.2 nmol/g tissue in the cortex. We assumed that founder mice with massive glycine accumulations died at an early age, whereas founder mice with no or moderate glycine accumulations survived. The remaining 10 founder mice grew normally and were fertile. These founder mice were mated with wild-type C57BL/6 mice, and their F_1 offspring were screened for brain glycine content. The mouse line with the highest glycine content had 1.36±0.06 μmol glycine per gram of tissue in the cerebral cortex (Figure 2A), in which glycine content in the striatum was also significantly high (Figure 2B). GCS activity in the mouse cerebrum was 0.04±0.01 nmol of CO_2 formed per milligram protein per hour, which was 29% of that of control C57BL/6 mice (0.14±0.03). This mouse line was designated low GCS. Histological examination revealed no abnormality in either high-GCS or low-GCS mice (data not shown).

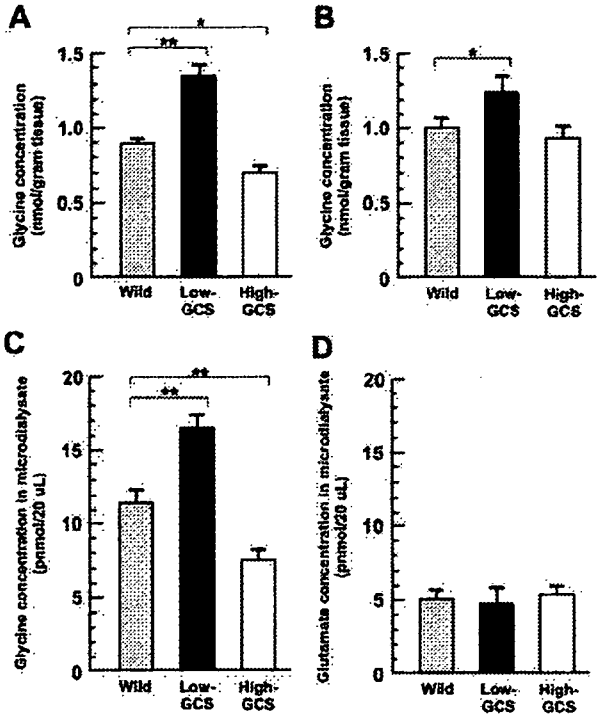

Figure 2. Glycine concentrations in high-GCS, low-GCS, and control C57BL/6 mice. Glycine contents in homogenate samples from the cerebral cortex (A) and striatum (B) were measured in the 3 mouse groups (n=6–8). Extracellular glycine (C) and glutamate (D) concentrations were analyzed by an in vivo microdialysis method. The extracellular glycine concentration was significantly higher ($P<0.01$) in low-GCS mice and significantly lower ($P<0.01$) in high-GCS mice compared with controls, whereas the extracellular glutamate concentration was not significantly different among the 3 mouse lines. *$P<0.05$, **$P<0.01$.

Basal Concentrations of Extracellular Amino Acid Neurotransmitters

Glycine concentrations in microdialysates were 11.7±1.0, 7.3±0.9, and 16.6±1.0 pmol/20 μL in wild-type C57BL/6, high-GCS, and low-GCS mice, respectively (Figure 2C). Extracellular glycine concentrations were therefore estimated as 1.0±0.1, 1.4±0.1, and 0.6±0.1 μmol/L in wild-type, low-GCS, and high-GCS mice, respectively, based on the sampling efficiency of our microdialysis system. Glutamate concentrations in microdialysates of wild-type C57BL/6, high-GCS, and low-GCS mice were 5.0±0.8, 5.4±0.7, and 4.8±1.5 pmol/20 μL, respectively (Figure 2D), which corresponded to 0.4±0.1, 0.5±0.1, 0.4±0.1 μmol/L, respectively, in extracellular glutamate concentration. The glycine and glutamate concentrations in wild-type mice showed good agreement with those in a previous report.[6] The extracellular concentration of glycine was significantly ($P<0.01$) higher or lower in low-GCS or high-GCS mice, respectively, compared with wild-type mice. No significant difference was observed among the 3 mouse lines in terms of extracellular concentrations of glutamate, taurine, alanine, or γ-aminobutyric acid (GABA), as shown in Figures 3C through 3E.

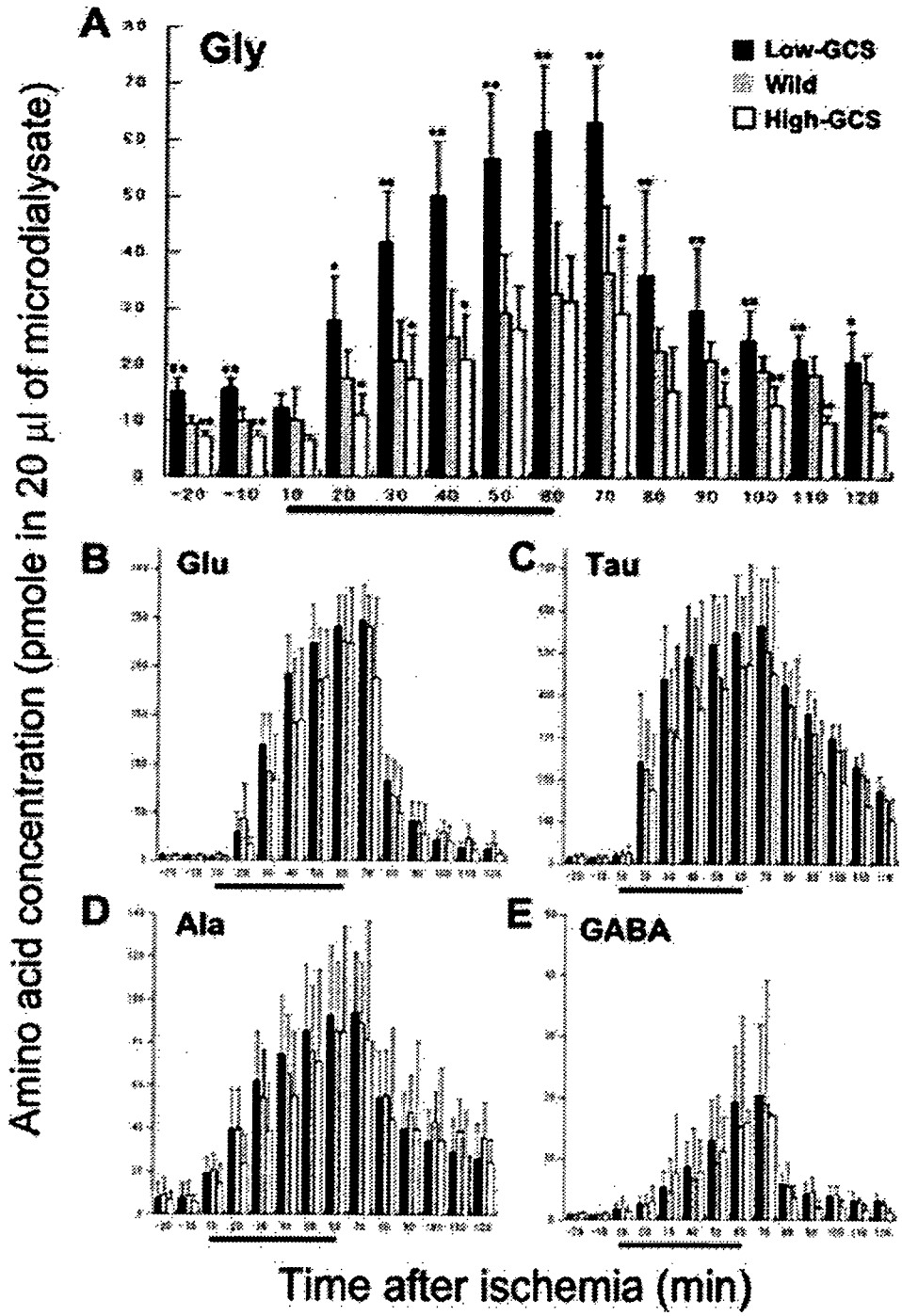

Figure 3. Extracellular concentrations of amino acid neurotransmitters in focal ischemia. A, The glycine concentration was significantly higher and lower in the low-GCS (n=10) and high-GCS (n=10) group, respectively, compared with controls (n=10). There were no significant differences in extracellular concentrations of glutamate (B), taurine (C), alanine (D), or GABA (E) among the 3 groups. The horizontal bar stands for the MCA occlusion period (60 minutes). Values are mean±SD. $^{*}P<0.05$, $^{**}P<0.01$.

Profiles of Extracellular Amino Acid Concentrations in MCA Occlusion

The glycine concentrations in all groups increased significantly at 20 minutes after MCA occlusion and reached their peak at 10 minutes after reperfusion (Figure 3A). The peak concentrations were 63.4±10.0, 36.6±12.0, and 31.5±7.9 pmol/20 μL in low-GCS, C57BL/6, and high-GCS mice, respectively. During and after MCA occlusion, glycine concentrations were persistently higher in low-GCS mice and lower in high-GCS mice compared with control mice. The glutamate concentrations were elevated in all 3 groups at 20 minutes after MCA occlusion and eventually reached their peak (247.7±35.9, 241.2±31.0, and 165.41±92.0 pmol/20 μL in low-GCS, C57BL/6, and high-GCS mice, respectively) at 10 minutes after reperfusion (Figure 3B). No significant difference in glutamate concentration was observed among the 3 groups

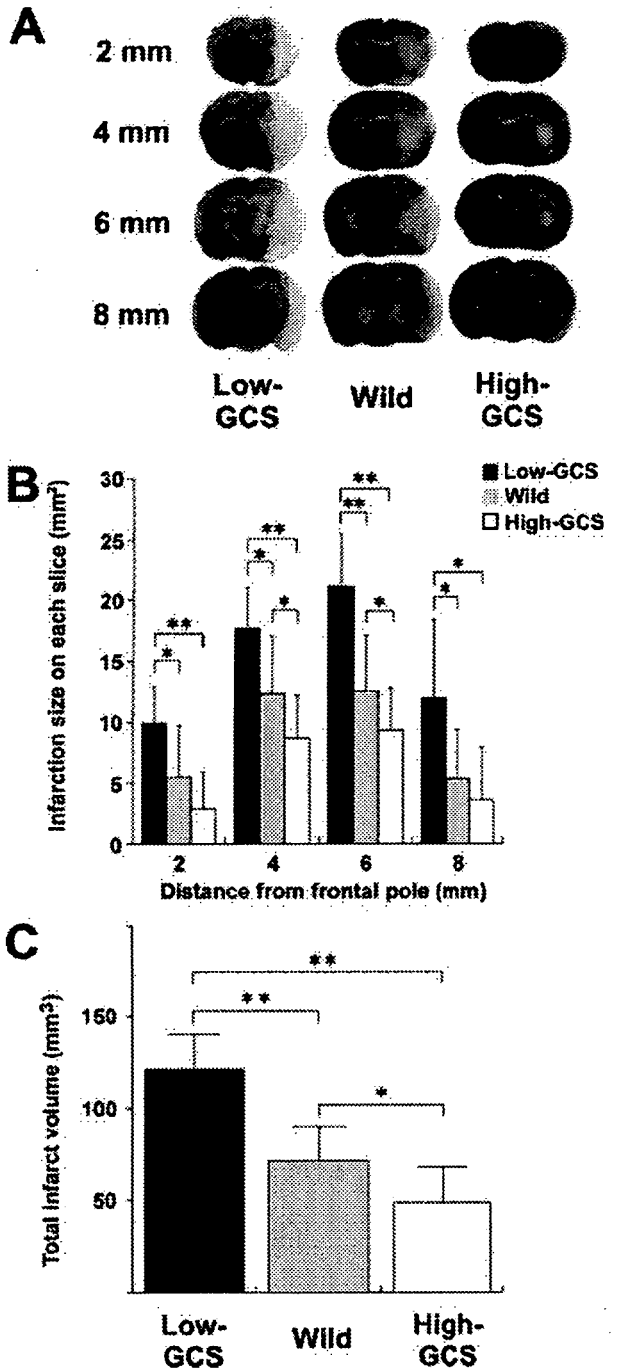

Figure 4. Evaluation of brain injury after MCA occlusion in low-GCS, high-GCS, and control C57BL mice. A 2-mm slice of brain sample was stained with triphenyltetrazolium chloride for visualization of the infarct region (white). Representative photographs of each mouse group (n=10) are shown (A). Infarct area (in mm^2) in each slice was measured (B). C, The infarct volume (in mm^3) in low-GCS mice was 69.8% larger than that of control mice. The infarct volume in high-GCS mice was 46.4% smaller than that of controls. Values are mean±SD. $^*P<0.05$, $^{**}P<0.01$.

throughout the experiments. MCA occlusion caused significant elevations of extracellular concentrations of taurine, alanine, and GABA (Figures 3C through 3E). There were no significant differences in extracellular taurine, alanine, or GABA concentrations among 3 mouse groups at each time point.

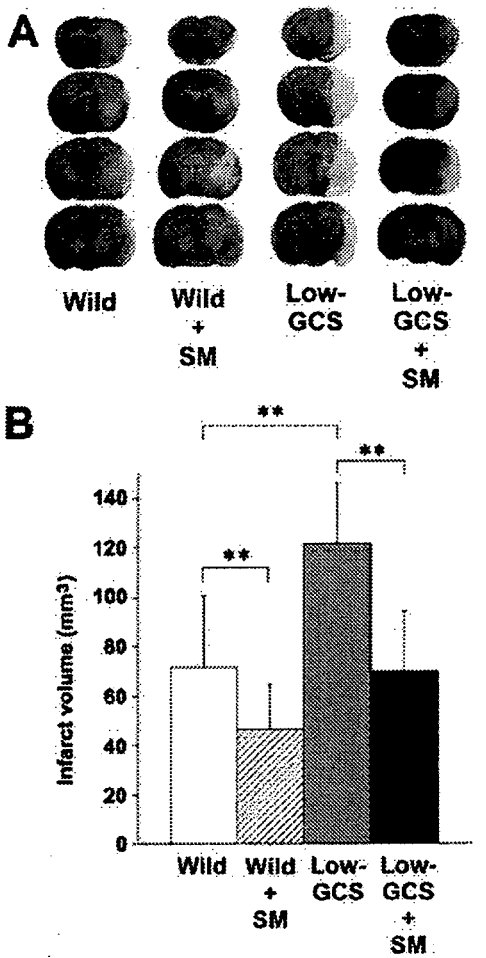

Figure 5. Effect of an NMDA receptor glycine site antagonist on cerebral infarction. Vehicle or SM-31900 (SM; 10 mg/kg IV) was administered twice at 30 and 10 minutes to wild-type C57BL/6 and low-GCS mice before MCA occlusion. A, Coronal brain slices were prepared from each mouse and then stained with triphenyltetrazolium chloride. B, Infarct volume was significantly reduced by SM-31900 administration in the control mice and more markedly in low-GCS mice. Mean±SD of each mouse group (n=6) is shown. $^{**}P<0.01$.

Infarct Size

In C57BL/6 control mice, infarct areas were mainly in the cortex and striatum (Figure 4A). The infarct areas extended to the whole MCA territory in low-GCS mice, whereas the areas were confined to the striatum in high-GCS mice. The infarct area in low-GCS mice was significantly larger than that of control mice in all slices, whereas the area of 4- and 6-mm slices was significantly smaller in high-GCS mice compared with controls (Figure 4B). As shown in Figure 4C, infarct volume in low-GCS mice after MCA occlusion was significantly increased by 69%, and that in high-GCS mice was significantly reduced by 21% compared with wild-type mice (low-GCS mice, 121.6±19.0 mm^3; control C57BL/6 mice, 71.6±29.1 mm^3; high-GCS mice, 56.5±7.9 mm^3).

Effect of the NMDA Receptor Glycine Site Antagonist SM-31900 on Infarct Size

Compared with vehicle-treated mice, infarct regions in the striatum and cortex were smaller in the SM-31900–treated

group in both low-GCS and control mice (Figure 5A). Pretreatment with SM-31900 significantly reduced infarct volume in C57BL/6 and low-GCS mice by 35% and 42%, respectively (control C57BL/6, 46.3 ±18.6 mm^3; low-GCS mice, 69.8±24.4 mm^3; Figure 5B). Physiological parameters during ischemic experiment are summarized in supplemental Table I, available online at http://stroke.ahajournals.org.

Discussion

We generated 2 transgenic mouse lines with genetically altered GCS activities, ie, high-GCS and low-GCS mice, and examined neural injury after MCA occlusion by monitoring concentrations of extracellular amino acids. Low-GCS mice had higher extracellular glycine concentrations and larger infarct volumes than did control mice. In sharp contrast, high-GCS mice had lower extracellular glycine levels and smaller infarct volumes. In the development of ischemic injury, a high extracellular concentration of glutamate is known to be neurotoxic,[2,21] whereas GABA plays a neuroprotective role.[22] In our experiments, no significant differences in extracellular glutamate or GABA concentrations were observed among the 3 mouse groups with distinct extracellular glycine concentrations. These results demonstrated a direct correlation between neuronal injury and extracellular glycine concentration, which is maintained by the GCS.

Glycine plays 2 important roles in the central nervous system: that of an inhibitory neurotransmitter and that of a modulator of excitation at the NMDA receptor. The infarct volume in low-GCS mice was markedly reduced by administration of an antagonist of the NMDA receptor glycine site. One possible explanation for this result is that low GCS activity affected ischemic damage mainly via the NMDA receptor. Lower GCS activity caused a higher extracellular glycine concentration, which resulted in overexcitation of NMDA receptors, leading to more severe ischemic injury. If SM-31900 had completely blocked the glycine site of the NMDA receptor, then infarct volume in SM-31900–treated wild-type mice would have been similar to that of SM-31900–treated, low-GCS mice. However, infarct volume in SM-31900–treated, low-GCS mice was similar to that of untreated, wild-type mice (Figure 5), which may suggest partial blocking of the glycine site by SM-31900 or the presence of another neuroprotective effect of SM-31900 that remains unidentified. At this moment, we cannot exclude the possibility that the altered GCS activity affected neural injury via inhibitory glycine receptors. Further study is required to understand the mechanism underlying a direct correlation between ischemic injury and extracellular glycine concentrations.

It is an old but still open question whether the glycine site of the NMDA receptor is saturated under physiological conditions.[23,24] Glycine is normally present in brain interstitial space at a concentration of 4 μmol/L in the cortex and 1 μmol/L in the striatum.[6,25] The NMDA-associated glycine-binding site is fully saturated at a glycine concentration of <1 μmol/L, suggesting that the glycine site of the NMDA receptor should be saturated under physiological conditions.[5] In line with these results, high extracellular glycine concentrations failed to potentiate NMDA-evoked depolarization in vivo by microdialysis with extracellular field potential recording.[7] Many in vivo studies have nevertheless demonstrated protective effects of NMDA glycine site antagonists.[9,24] In this study, we showed that infarct volume was larger in mice with higher extracellular glycine concentrations and that neural injury was ameliorated by an NMDA glycine site antagonist. Recently, we found that low-GCS mice had behavioral abnormalities such as hyperactivity and increased aggression. These phenotypes resemble the symptoms of patients with a mild form GE, who do not manifest neonatal seizures or coma but instead have behavioral abnormalities.[26] Thus far, these observations support the notion that the glycine-binding site of the NMDA receptor is not functionally saturated under physiological conditions and that the NMDA receptor could respond to changes in extracellular glycine concentrations.

Extracellular glycine reached its highest peak during MCA occlusion in low-GCS mice compared with controls (Figure 3A). Ischemia-induced acidosis leads to dysfunction of the glycine transporter, which triggers an efflux of intracellular glycine into the extracellular space.[27] The higher peak was probably due to a higher intracellular glycine content in the striatum in low-GCS mice (Figure 2B). The peak glycine level in high-GCS mice was not lower than that in controls 50 to 60 minutes after MCA occlusion, which may be explained by the fact that the glycine content in the striatum did not significantly differ between high-GCS and wild-type mice (Figure 2B). The elevated glycine level was normalized more rapidly in high-GCS mice compared with low-GCS and wild-type mice (Figure 3). Total glycine release during the first 2 hours after ischemia may affect the extent of ischemic injury rather than the glycine concentration at each time point.

An antagonist of the glycine site of the NMDA receptor, SM-31900, ameliorated ischemic injury in high-GCS mice, in accordance with a previous report that SM-31900 attenuated neuronal injury in a rat model of focal ischemia.[19] A number of antagonists for the glycine site of the NMDA receptor have been developed to date.[9] Clinical trials with some of the antagonists have been performed, but so far, these have proven unsuccessful. The infarct size in high-GCS mice (56.5±7.94 mm^3) was comparable to that of SM-31900–treated, wild-type C57BL/6 mice (46.3±18.6 mm^3) as shown in Figures 4C and 5B, suggesting that the enhancement of GCS activity has a similar neuroprotective effect. If a small molecule that enhances GCS activity were to become available, it could be used as a neuroprotective drug for various NMDA receptor–related neurodegenerative disorders. The low-GCS and high-GCS mouse lines established in the current study would be valuable tools for studying the effect of extracellular glycine concentrations in vivo.

Sources of Funding

This work was supported by a grant from the Ministry of Education, Culture, Sports, Science, and Technology in Japan (No.17591067 to S.K. and No.17591497 to H.K.).

Disclosures

None.

References

1. Graham SH, Shiraishi K, Panter SS, Simon RP, Faden AI. Changes in extracellular amino acid neurotransmitters produced by focal cerebral ischemia. *Neurosci Lett.* 1990;110:124–130.

2. Lipton SA, Rosenberg PA. Excitatory amino acids as a final common pathway for neurologic disorders. *N Engl J Med.* 1994;330:613–622.
3. Betz H, Langosch D, Hoch W, Prior P, Pribilla I, Kuhse J, Schmieden V, Malosio ML, Matzenbach B, Holzinger F, et al. Structure and expression of inhibitory glycine receptors. *Adv Exp Med Biol.* 1991;287:421–429.
4. Johnson JW, Ascher P. Glycine potentiates the NMDA response in cultured mouse brain neurons. *Nature.* 1987;325:529–531.
5. Newell DW, Barth A, Ricciardi TN, Malouf AT. Glycine causes increased excitability and neurotoxicity by activation of NMDA receptors in the hippocampus. *Exp Neurol.* 1997;145:235–244.
6. Shimizu-Sasamata M, Bosque-Hamilton P, Huang PL, Moskowitz MA, Lo EH. Attenuated neurotransmitter release and spreading depression-like depolarizations after focal ischemia in mutant mice with disrupted type I nitric oxide synthase gene. *J Neurosci.* 1998;18:9564–9571.
7. Obrenovitch TP, Hardy AM, Urenjak J. High extracellular glycine does not potentiate *N*-methyl-D-aspartate-evoked depolarization in vivo. *Brain Res.* 1997;746:190–194.
8. Zhao P, Qian H, Xia Y. GABA and glycine are protective to mature but toxic to immature rat cortical neurons under hypoxia. *Eur J Neurosci.* 2005;22:289–300.
9. Jansen M, Dannhardt G. Antagonists and agonists at the glycine site of the NMDA receptor for therapeutic interventions. *Eur J Med Chem.* 2003;38:661–670.
10. Patel J, Zinkand WC, Thompson C, Keith R, Salama A. Role of glycine in the NMDA-mediated neuronal cytotoxicity. *J Neurochem.* 1990;54: 849–854.
11. Zafra F, Aragon C, Gimenez C. Molecular biology of glycinergic neurotransmission. *Mol Neurobiol.* 1997;14:117–142.
12. Sato K, Yoshida S, Fujiwara K, Tada K, Tohyama M. Glycine cleavage system in astrocytes. *Brain Res.* 1991;567:64–70.
13. Sakata Y, Owada Y, Sato K, Kojima K, Hisanaga K, Shinka T, Suzuki Y, Aoki Y, Satoh J, Kondo H, Matsubara Y, Kure S. Structure and expression of the glycine cleavage system in rat central nervous system. *Brain Res Mol Brain Res.* 2001;94:119–130.
14. Kikuchi G. The glycine cleavage system: composition, reaction mechanism, and physiological significance. *Mol Cell Biochem.* 1973;1: 169–187.
15. Kure S, Kato K, Dinopoulos A, Gail C, Degrauw TJ, Christodoulou J, Bzduch V, Kalmanchey R, Fekete G, Trojovsky A, Plecko B, Breningstall G, Tohyama J, Aoki Y, Matsubara Y. Comprehensive mutation analysis of GLDC, AMT, and GCSH in nonketotic hyperglycinemia. *Hum Mutat.* 2006;27:343–352.
16. Kure S, Narisawa K, Tada K. Structural and expression analyses of normal and mutant mRNA encoding glycine decarboxylase: three-base deletion in mRNA causes nonketotic hyperglycinemia. *Biochem Biophys Res Commun.* 1991;174:1176–1182.
17. Niwa H, Yamamura K, Miyazaki J. Efficient selection for high-expression transfectants with a novel eukaryotic vector. *Gene.* 1991;108: 193–199.
18. Kamii H, Kinouchi H, Sharp FR, Koistinaho J, Epstein CJ, Chan PH. Prolonged expression of hsp70 mRNA following transient focal cerebral ischemia in transgenic mice overexpressing CuZn-superoxide dismutase. *J Cereb Blood Flow Metab.* 1994;14:478–486.
19. Ohtani K, Tanaka H, Ohno Y. SM-31900, a novel NMDA receptor glycine-binding site antagonist, reduces infarct volume induced by permanent middle cerebral artery occlusion in spontaneously hypertensive rats. *Neurochem Int.* 2003;42:375–384.
20. Kinouchi H, Epstein CJ, Mizui T, Carlson E, Chen SF, Chan PH. Attenuation of focal cerebral ischemic injury in transgenic mice overexpressing CuZn superoxide dismutase. *Proc Natl Acad Sci U S A.* 1991;88: 11158–11162.
21. Choi DW, Rothman SM. The role of glutamate neurotoxicity in hypoxic-ischemic neuronal death. *Annu Rev Neurosci.* 1990;13:171–182.
22. Madden KP. Effect of γ-aminobutyric acid modulation on neuronal ischemia in rabbits. *Stroke.* 1994;25:2271–2274; discussion 2274–2275.
23. Wood PL. The co-agonist concept: is the NMDA-associated glycine receptor saturated in vivo? *Life Sci.* 1995;57:301–310.
24. Danysz W, Parsons AC. Glycine and *N*-methyl-D-aspartate receptors: physiological significance and possible therapeutic applications. *Pharmacol Rev.* 1998;50:597–664.
25. Globus MY, Busto R, Martinez E, Valdes I, Dietrich WD, Ginsberg MD. Comparative effect of transient global ischemia on extracellular levels of glutamate, glycine, and γ-aminobutyric acid in vulnerable and nonvulnerable brain regions in the rat. *J Neurochem.* 1991;57:470–478.
26. Dinopoulos A, Kure S, Chuck G, Sato K, Gilbert DL, Matsubara Y, Degrauw T. Glycine decarboxylase mutations: a distinctive phenotype of nonketotic hyperglycinemia in adults. *Neurology.* 2005;64:1255–1257.
27. Swanson RA, Ying W, Kauppinen TM. Astrocyte influences on ischemic neuronal death. *Curr Mol Med.* 2004;4:193–205.